

**Apo A-1 mimetic peptide, L-4F prevents insulin resistance through
increased HO-1 and pAMPK in obese mice**

Stephen J. Peterson^{1,2}, George Drummond¹, Dong Hyun Kim¹, Ming Li¹,
Vincenzo Positano³, Luca Vanella¹, Francesco Piccolomini¹, Luigi F. Rodella¹,
Amalia Gastaldelli³, Claudia Kusmic³, Antonio L'Abbate^{3,4}, Attallah Kappas^{1,5},
and Nader G. Abraham^{1,2}

Departments of Pharmacology¹ and Medicine², New York Medical College,
Valhalla, NY, 10595, ³CNR Institute of Clinical Physiology and ⁴Scuola Superiore
Sant'Anna, Pisa, Italy
and ^{1,5}The Rockefeller University, NY 10021

Abbreviated Title: L-4F moderates obesity and diabetes

Address correspondence and reprint requests to:

Dr Attallah Kappas, The Rockefeller University, 1230 York Avenue, NY, NY
10021, Tel: 212-327-8494 **Or** Dr. Nader G. Abraham, Professor of Pharmacology
and Medicine, New York Medical College, Valhalla, NY 10595, Tel: (914) 594-
4132, FAX: 914 594-4119 E-mail: nader_abraham@nymc.edu

ABSTRACT

We investigated the mechanisms by which L-4F, an apolipoprotein A-1 mimetic peptide, reduces obesity and diabetes in obese (ob) diabetic mice. We hypothesized that L-4F reduces vascular dysfunction via an increase in pAMPK and pAKT in both ob diabetic mice and human stem cells. Mice, ob and lean, were fed a normal diet until 9 weeks of age, when all ob mice had established diabetes treated with L-4F. Food intake, blood insulin, glucose levels, adipocyte stem cells and pAMPK, pAKT, SREBP-1 and insulin receptors were determined. Subcutaneous fat tissue (SAT) and visceral adipose tissue (VAT) by magnetic resonance imaging (MRI). MRI showed that both SAT and VAT global volumes decreased in ob-L-4F-treated animals ($p < 0.05$ compared to ob controls). L-4F treatment decreased hepatic lipid content, increased adipocytes of small cell size ($p < 0.05$), increased insulin sensitivity ($p < 0.04$) and phosphorylation of insulin receptors. L-4F treatment decreased nuclear expression of SREBP-1 ($p < 0.01$). L-4F-mediated increased levels of pAKT and pAMPK was prevented by LY294002 resulting in a significant increase in serum glucose levels, $p < 0.001$. The anti-obesity effects of L-4F are manifest by a decrease in visceral fat content and reciprocal increases in HO-1, adiponectin, pAMPK, pAKT, restoration of vascular function and phosphorylation of insulin receptors.

Supplementary key words: Diabetes; adiponectin; adiposity; apolipoprotein A-I mimetic peptides; heme oxygenase-1; insulin receptor; insulin sensitivity; pAMPK; obesity; endothelial dysfunction

Abbreviations: ApoA-1, apolipoprotein A-1; HO, heme oxygenase; LDL; low density lipoprotein; HDL, High density lipoprotein; CVD; Cardiovascular disease; LMW, low molecular weight; HMW, high molecular weight; MSC, mesenchymal stem cells.

INTRODUCTION

Apolipoprotein A1 mimetic peptides, synthesized from either D (D-4F) or L (L-4F) amino acids enhance the ability of high density lipoprotein (HDL) to protect low density lipoprotein (LDL) against oxidation in atherosclerotic animals (1-3). Prior studies show that oral administration of D-4F can reduce atherosclerotic disease independent of cholesterol levels (2, 3). Treatment with D-4F causes HDL to become anti-inflammatory, stimulates HDL-mediated cholesterol efflux and reverses cholesterol transport from macrophages (1, 2). L-4F and D-4F improve vascular function and restore the balance between nitric oxide (NO) and superoxide (O_2^-) anions and increase HO-1 and peNOS levels (4-7). Using a sickle cell disease model, Ou et al. demonstrated that apolipoprotein A1 can improve vasoreactivity in LDL-receptor null mice (5). These data indicate an antioxidant effect of apolipoprotein A1, D-4F.

Insulin resistance is the hallmark of type 2 diabetes and its associated cardiovascular disease (CVD) (8, 9). Once hyperglycemia is established, an increase in ROS occurs resulting in a progressive deterioration in vascular function and an elevation of the levels of inflammatory cytokines by adipose tissue (10). Obesity is also a risk factor for CVD and diabetes in humans and in animals (11, 12). Obesity and hyperglycemia are independent predictors of cardiovascular disease (13, 14). Obesity and diabetes are strongly associated with endothelial dysfunction (6, 15-19) as manifested by increases in lipolysis, hepatic triglyceride secretion and the sterol-regulatory element binding protein-1 (SREBP-1) (20). SREBPs are major transcription factors that regulate genes

involved in fatty acid and cholesterol synthesis and are regulated by pAMPK and pAKT in ob mice (20). Additionally, activation of the endocannabinoid receptor-1 (CB1 receptor), a regulatory protein linked to abnormal glucose levels and obesity, was shown to increase the hepatic lipogenic transcription factor, SREBP-1, and fatty acid synthesis (21). In visceral adipose tissue, increased CB1 receptor activity leads to a decrease in adiponectin and an increase in lipogenesis both of which contribute to insulin resistance.

Hyperglycemia has been linked to endothelial cell injury and vascular dysfunction through decreases in pAKT, HO-1 and peNOS (6, 15, 22, 23). pAMPK and pAKT are required for increased levels of peNOS to prevent the detrimental perturbations associated with elevated levels of insulin, shear stress and VEGF (24-27). In addition, chronic increased expression of the HO-1-adiponectin-axis decreased obese-mediated inflammation, TNF and, IL-6 levels and increased insulin sensitivity (12, 28, 29) pAKT is required for vascular homeostasis, appropriate levels of pAKT are needed for normal vascular function (30), presumably through crosstalk with pAMPK in vascular cells (31-33).

Induction of HO-1 protein is associated with a marked increase in the serum levels of adiponectin and a decrease in the levels of the inflammatory cytokines IL-1, IL-6, and TNF (12, 34). A spectrum of agents have been shown to be potent inducers of HO-1 in endothelial cells including apolipoprotein A-1, D- and L-4F peptides, probucol, simvastatin, and lovastatin (6, 12, 35-39). In the present study we examined the mechanism of Apo A1-mimetic, L-4F, on vascular

expression of pAMPK and AKT, insulin receptor phosphorylation in relation to visceral fat and adipogenesis and vascular function in obese diabetic mice.

MATERIALS AND METHODS

Animal protocols

Male obese (ob) mice (B6v-Lep ob/J) were purchased from Harlan (Chicago, IL) at the age of 7 weeks and used at 8 weeks of age. Age- and sex-matched lean mice (B6.V, lean, Harlan, Chicago, IL) served as controls. Mice were fed a normal chow diet and had free access to water. Body weight of ob and lean mice at the beginning of the treatment were 34 ± 5 g and 26 ± 3 g, respectively. Glucose levels were (248 ± 21 and 126 ± 14 mg/dL) for ob and lean mice respectively. Glucose monitoring was performed using an automated analyzer (Life scan Inc., Milpitas, CA). Beginning at 9 weeks of age when all ob mice had established diabetes, L-4F (i.e. Ac-D-W-F-K-A-F-Y-D-K-V-A-E-K-F-K-E-A-F-NH₂) synthesized from L-amino acids as previously described (40) was injected at a dose of 200 μ g/100 gm daily in 200 μ l vehicle), or vehicle (ABCT: ammonium bicarbonate buffer at pH 7.4 containing 0.01% Tween²⁰) were administered intraperitoneally (i.p.) for 6 weeks. Blood was collected (50-100 μ l) from the tail vein of anesthetized ob mice following administration of either L-4F or vehicle. L-4F treated ob mice were divided into two groups, one treated with L-4F and the P13 kinase AKT inhibitor, LY294002, (cell signaling, Technology, Boston, MA) 2-(4-morpholinyl)-8-phenyl-4H-1-benzopyran-4-HCl, which was dissolved in DMSO and diluted with PBS and injected i.p. at a dose of 100 mg/kg, three times a week for the last three weeks of the study (41). The second group of ob-L-4F-treated mice were treated with the same volume of vehicle (PMSO+PBS) without LY294002. Six groups of animals were studied: A) lean, B)

lean-L-4F, C) lean-L-4F-LY-294002, D) ob control, E) ob-L-4F, and F) ob-L-4F-LY294002. Food intake did not change in the mice in any treatment group. The Animal Care and Use Committee of New York Medical College approved all experiments.

Magnetic resonance imaging (MRI) and magnetic resonance spectroscopy (MRS)

Subcutaneous fat tissue (SAT) and visceral fat tissue (VAT) were determined by MRI while hepatic fat was determined by magnetic resonance spectroscopy (MRS). Mice were imaged in a GE (USA) excite 1.5T scanner using a knee coil with a T1-weighted spin-echo pulse sequence (TEC 9.0 ms, TR=540ms, NEX=4, FOVO 8 x8 cm), image size 224X192 pixels. The whole chest and abdomen of each mouse were covered with axial slices (thickness 3 mm, no spacing). Acquired images underwent semi-automatic segmentation of SAT and VAT using the previously validated HIPPO FAT[®] tool (42-44).

The software computed three masks (background, fat, and non-fat tissues) using a fuzzy clustering segmentation. After this step, external and internal SAT boundaries were defined by an active contour algorithm that exploited the previously computed masks as external force maps. A third contour was computed surrounding the area where VAT was present together with other tissues. VAT itself was assessed by the automated analysis of the signal histogram in the visceral region previously defined, by identifying the second peak of the signal histogram. This provided whole body volume (including the

skeletal and soft tissues), total fat, SAT, and VAT volumes, as well as VAT/SAT ratio and fat/body volume ratio.

Liver lipid measurements

Localized ^1H Magnetic Resonance Spectroscopy (MRS) of the liver was acquired on a 1.5 T magnetic resonance imaging scanner (EXCITE, General Electric, USA). The liver slice with the largest gross dimensions was chosen for the MRS study. MRS for water and fat quantification was accomplished using a point resolved spectroscopy sequence. After line broadening, phase and baseline correction, the peak area of the water at 4.77 ppm, and fat resonance (FR) at 1.40 ppm were measured. Quantification of the fat content was done by comparing the area of the FR with that of the unsuppressed water. Spectroscopic data were processed using the NUTS software. Hepatic fat percentage was calculated by dividing FR by the sum of FR and peak area of water. This technique is highly reproducible, with a coefficient of variation less than 2% when slices were studied on eight separate occasions.

Determination of HO-1, adipocyte cell size, SREBP-1, HO-1 and CB1

Subcutaneous adipose tissue and renal, liver and aortic visceral fat tissue collected from untreated ob mice and L-4F-treated ob mice (n=8 mice per group) were prepared for morphological analysis. Samples were fixed in 4% paraformaldehyde for 24h, cut into small pieces and embedded in paraffin for

histological analysis. The samples were cut by microtome (5 μm thick), mounted on D-polylysinated glass slides, deparaffinized in xylene and stained with haematoxylin and eosin for the evaluation of adipocyte size or processed for CB-1 or HO-1 immunohistochemistry. Immunostaining for CB-1 was carried out using a goat polyclonal anti-CB-1 and SREB1 primary antibodies (7) (Santa Cruz Biotechnology, Santa Cruz, CA) and HO-1 immunostaining was carried out using a rabbit polyclonal anti-HO-1 primary antibody (Stressgen Bio reagents, Victoria, BC, Canada). For each experimental group, five sections per animal were stained. Sections were immersed in 3% hydrogen peroxide and diluted in methanol for 30 min to quench endogenous peroxidase activity. The sections were pre-incubated with 3% horse serum for 60 min followed by primary antibody anti-CB-1 diluted 1:125 for 2 h at 37°C. The sections were then washed in TBS (0.1 M), incubated 30 min at room temperature, with biotinylated horse anti-goat immunoglobulin (Vector Laboratories, Burlingame, CA) and then incubated for 30 min at room temperature with avidin-biotin-horseradish peroxidase complex (ABC complex, Vector Laboratories, Burlingame, CA). The reaction product was visualized using hydrogen peroxide and diaminobenzidine (DAB) (Sigma) as the chromogen. All slides were dehydrated and mounted in DPX (Sigma, St. Louis, USA). Negative controls primary antibody with non-immune serum, revealed no signal.

Evaluation of CB-1 and HO-1 immunoassaying analysis

CB-1 and HO-1 staining intensity was computed as integrated optical density (IOD). Digitally fixed images of the slices (n=5 per animal) at 20X magnification were analyzed using an optical microscope (Olympus, Germany) equipped with an image analyzer (Image Pro Plus, Immagini e Computer, Milan, Italy). For quantitative analysis, IOD was calculated for arbitrary areas, measuring three fields with the same area for each section.

Evaluation of adipocyte size analysis

Digital images of adipose tissue sections were captured using a light microscope (Olympus, Germany) at 20X magnification. For each group, three fields from each of five different haematoxylin-eosin stained sections per animal were analyzed. Individual adipocyte areas (μm^2) within each field were determined using image analysis software (Image Pro Plus, Immagini e Computer, Milan, Italy). For the quantitative analysis, adipocyte areas were calculated in arbitrary fields, measuring fifty adipocytes for each section.

Western blot analysis of liver, kidney and adipocyte stem cells for HO-1, AMPK, pAMPK, AKT, pAKT and insulin receptor phosphorylation

At sacrifice, subcutaneous and visceral fat in the abdomen (the visible mesenteric fat, fat around the liver, fat around the kidney and fat around the spleen) were dissected free, pooled for each mouse and used to isolate adipocyte stem cells. Specimens were stored at -140°C until assayed. Frozen

liver, kidney, heart and fat tissues were pulverized under liquid nitrogen and placed in a homogenization buffer (mmol/l: 10 phosphate buffer, 250 sucrose, 1 EDTA, 0.1 PMSF and 0.1% v/v tergitol, pH 7.5). Homogenates were centrifuged at 27,000xg for 10 min at 4°C, supernatant was isolated and protein levels were visualized by immunoblotting with antibodies. Antibodies against, AMPK, pAMPK, AKT, and pAKT were obtained from Cell Signaling Technology, Inc. (Beverly, MA). Antibodies were prepared by dilution of HO-1, pAMPK, pAKT and insulin receptor as we described previously (12, 28, 29).

Glucose tolerance test

After a 12 hour fast, mice were injected i.p. with glucose (2.0g/kg body weight). Blood samples were taken at various time points (0-120 min), for measurement of blood glucose levels.

Human bone marrow-derived mesenchymal stem cells and adipocytes

Frozen bone marrow mononuclear cells were purchased from Allcells (Allcells, Emeryville, CA). After thawing the cells, mononuclear cells were cultured as previously described (12, 28, 29).

Adipogenic differentiation of human MSCs and effect of L-4F

Adipogenic differentiation of human MSCs was induced by incubation in an adipogenesis induction medium (DMEM-high glucose (45, 46), supplemented with 10 µg/mL of insulin, 1 µmol/L of dexamethasone, 0.2 mmol/L of

indomethacin, 10% FBS and 1% antibiotic–antimycotic solution). The medium was changed every 3-4 days (45, 46), in the presence of vehicle alone or vehicle containing L-4F. At 50% confluence, L-4F and vehicle solutions were added, HO-1, adiponectin, pAMPK and adipogenesis was measured using oil red O as previously described (12). MSC-derived adipocytes were treated with 7.5 μ M LY294002, a dose effective in inhibiting P 1-3 Kinase/AKT (47).

Measurement of fiber diameter and fat deposits

Serial sections (8 μ m thick) were cut by cryostat and stained with hematoxylin-eosin, for morphological evaluation (measurement of diameter) and with Oil Red O staining for the analysis of fat deposits. Digital images were taken using a light microscope (Olympus Germany) and then analyzed with a software program (Image-Pro Plus 4.5.1, Milan Italy). Ten fibers from each muscle slice were randomly selected to estimate fiber diameter; fat deposits were evaluated through measurement of the percentage of Oil Red O stained area in 5 fields per randomly selected muscle sections. A total of 5 sections per animal were analyzed.

Adipocyte mesenchymal stem cell isolation from SAT and VAT of lean, ob and ob L-4F treated mice

To isolate mouse adipocyte mesenchymal stem cells (AMSC), adipose tissues were washed with phosphate-buffered saline (PBS) and digested at 37°C for 30 min with 0.075% type II collagenase (48). At 50% confluence, L-4F was

added as indicated in figures legends and HO-1 or adipogenesis was measured using oil red O staining (12).

Statistical analyses

Statistical significance between experimental groups was determined by the Fisher method of analysis of multiple comparisons ($p < 0.05$ was regarded as significant). For comparison between treatment groups, the null hypothesis was tested by either a single-factor ANOVA for multiple groups or unpaired t test for two groups. Data are presented as mean \pm SE except for cell size and IOD for SREBP-1 and CB1 which are presented as mean \pm SD. Differences between experimental groups were evaluated with ANOVA with Bonferroni corrections. Statistical significance was set at $p < 0.05$.

RESULTS

L-4F treatment reduces weight gain and fat content

We examined the effect of L-4F treatment on body weight and fat appearance. As seen in Figure 1, L-4F-treatment visibly reduced weight gain in ob mice. The final weights after 6 weeks of either vehicle or L-4F treatment were (53 ± 2.9 g and 43.2 ± 1.7 g, respectively, $p<0.05$). The L-4F mediated reduction of weight gain was reversible. When L-4F was discontinued at week 10, ob mice gained weight at a faster rate than ob vehicle treated animals (data not shown). As seen in Figure 1, visceral fat in obese mice was decreased by L-4F treatment.

Effect of L-4F on fat content determined by magnetic resonance imaging (MRI)

Visual inspection and dissection of visceral fat around various organs and dissection of subcutaneous fat provide semi-quantitative estimates of fat content. MRI was used to quantify SAT and VAT. As seen on Figure 2, global SAT and global VAT were significantly decreased, $p<0.05$ and $p<0.01$, respectively. The decrease in visceral fat was accompanied by a significant increase in adiponectin levels and a decrease in the levels of the inflammatory cytokine IL-1 β . Prior to treatment, adiponectin levels in the ob mice were 2.73 ± 0.51 $\mu\text{g/ml}$ compared to 4.76 ± 0.93 $\mu\text{g/ml}$ ($p<0.029$) in lean animals. L-4F treatment resulted in a significant increase ($p<0.01$) in the levels of serum adiponectin to 6.14 ± 1.49 $\mu\text{g/ml}$ in the ob mice. Obese mice exhibited a significant increase in serum IL-1 β

levels (123 ± 29 pg/ml) when compared to age-matched lean controls (48 ± 31 pg/ml), $p < 0.05$. L-4F treatment resulted in a significant ($p < 0.01$) decrease in serum IL-1 levels in the ob mice (39 ± 26 pg/ml) compared to untreated ob to levels seen in the lean mice confirming previous data (29).

L-4F treatment did not affect muscle weight or intramuscular Oil Red O staining

The weight of gastrocnemius muscle in lean mice, untreated ob mice, and L-4F-treated ob mice was 393 ± 46 mg, 350 ± 52 mg, and 356 ± 48 mg, respectively (Figure 3). As shown in Figure 3, L-4F treatment did not affect muscle fiber, fat content or muscle diameter. The diameters of muscle fibers for the lean, ob untreated, and L-4F treated mice were 50 ± 4.7 μm , 53 ± 4 μm and 51 ± 4 μm , respectively (Figure 3B). Intramuscular lipid droplets were several fold higher in ob compared to lean mice ($p < 0.005$) but were not different in ob mice treated with L-4F when compared to untreated ob mice (Figure 3D).

Effect of L-4F on adipocyte size and expression of CB1 and HO-1

Histological examination of SAT and VAT revealed that adipocyte cell size was significantly decreased (Figure 4). Adipocyte cell size in the subcutaneous fat of control ob mice was 52 ± 14 $\mu\text{m}^2 \times 100$ (Figure 4A). Adipocyte cell size was significantly lower in L-4F-treated ob mice, 42 ± 11 $\mu\text{m}^2 \times 100$, ($p < 0.05$). A similar reduction was seen with L-4F treatment in adipocyte cell size in visceral fat surrounding aortic tissue (Figure 4B). Adipocyte cell size was proportionally lower

in subcutaneous fat tissue. Adipocyte cell size in lean animals was $37\pm 9 \mu\text{m}^2 \times 100$ compared to lean mice treated with L-4F ($26\pm 7 \mu\text{m}^2 \times 100$) (Results not shown).

We examined the effect of L-4F treatment on CB1 expression in adipose tissue. The level of CB1 expression in SAT was significantly lower in L-4F-treated ob mice (595 ± 119 in control ob mice compared to 334 ± 98 in L-4F-treated ob mice; $p < 0.05$) (Figure 5). Similarly, the level of CB1 expression in VAT was significantly lower in L-4F-treated ob mice (788 ± 124 in control ob mice compared to 589 ± 153 in L-4F-treated ob mice; $p < 0.05$) (Figure 5).

L-4F treatment of ob mice increased HO-1 expression in both SAT and VAT (Figure 6), while it downregulated the CB1 receptors.

Effect of L-4F on Hepatic lipid content

Magnetic resonance imaging showed that fat constituted 40% of hepatic tissue in untreated ob mice but only 15% of hepatic tissue in ob mice treated with L-4F. For comparison, hepatic fat content in lean mice was less than 5% (Figure 7).

Effect of L4-F on SREBP-1

The effect of L-4F treatment on SREBP-1 expression and insulin signaling proteins was examined by immunostaining for SREBP-1 in renal tissues isolated from untreated ob and L-4F-treated ob animals. Staining was localized within the nuclear and cytoplasm compartments. SREBP-1 staining was strong in both

compartments in kidney from ob mice untreated (Figure 8, right panel). Optical density analysis of immunohistochemical staining provided quantification of the changes in SREBP-1 expression (Figure 8). The levels of SREBP-1 were increased ($p < 0.001$) in untreated ob mice when compared to lean animals. SREBP-1 levels were decreased to levels of lean animals after L-4F treatment (Figure 8). Western blot analysis showed that SREBP-1 was increased in the nuclear fraction of untreated ob mice and L-4F treatment prevented this SREBP-1 translocation to the nuclear compartment (data not shown).

Effect of L-4F on liver insulin receptor phosphorylation

Visceral fat depots drain into the portal circulation resulting in the elevation of the levels of free fatty acids, which has been implicated in the genesis of impaired insulin-signaling and decreased phosphorylation of the insulin receptor. We therefore examined the effect of L-4F treatment on liver insulin receptor phosphorylation in untreated ob and lean mice. Phosphorylation of insulin receptors at sites Tyr-972 and Tyr-1146 was examined as seen in Figure 9, insulin phosphorylation at sites 972 and 1146 was significantly decreased in untreated ob mice compared to lean animals and restored by L-4F treatment. Densitometry analysis showed that L-4F treatment increased the ratio of P-Tyr 972 and Tyr-1146 in L-4F-treated ob mice compared to untreated ob mice ($p < 0.01$) and the resulting levels were equal to or greater than those in lean mice (Figure 9).

Effect of AKT kinase inhibition on glucose levels.

Plasma glucose levels in ob mice treated with vehicle were significantly higher than those in ob mice treated with L-4F at all time points during the glucose tolerance test. Blood glucose levels in vehicle treated ob mice were significantly ($p < 0.001$) elevated after glucose administration at all time points (Figure 10A, upper panel). To clarify the role of pAKT and pAMPK as a downstream signal in insulin sensitivity, we examined the effect of LY294002 inhibition of pAKT by administration on glucose levels. As seen in Figure 10A, lower panel, LY294002 prevented the L-4F anti hyperglycemic effect resulting in increased glucose levels compared to L-4F treated ob mice.

Effect of L-4F on aorta AKT, pAKT, AMPK and pAMPK

As seen in Figure 10B, AKT in aorta tissue isolated from untreated ob mice was no different from that in lean mice or ob mice treated with L-4F. However, there were significant decreases in both pAKT and pAMPK in ob mice. L-4F treatment increased both pAKT and pAMPK protein levels compared to untreated ob mice. Densitometry analysis showed that pAKT were increased significantly in ob mice treated with L-4F, compared to non-treated ob mice, $p < 0.04$. Similar effects were seen on pAMPK signal protein (data not shown). Additionally, as seen in Figure 10 B, LY294002 administration prevented the increase in L-4F induced phosphorylation of not only AKT and AMPK. The

amount of non phosphorylated AKT or AMPK was unaffected by either L-4F or LY294002 treatment.

Effect of L-4F and inhibitors of AKT on adipogenesis

We also examined the effect of inhibition of pAKT by LY294002 on adipogenesis. As shown, (Figure 11A), treatment with LY294002 (7.5 μ M) increased oil red O staining in L-4F treated cells. LY294002 alone did not significantly affect cell viability (data not shown). L-4F increased the number of small adipocyte cells in a dose-dependent manner (data not shown). Addition of LY294002 decreased the number of small lipid droplets and increased the number of large lipid droplets. L-4F in combination with LY294002 significantly increased the total adipocyte number and decreased the average cell size (data not shown). Figure 11B shows the levels of adipocytes cultured in the presence and absence of L4-F. L4-F significantly decreased adipogenesis ($p < 0.05$) as measured by oil red O staining. Incubation of LY294002 with L4F prevented the L4F mediated decrease in oil red O staining.

Figure 11 C shows the effect of the quantitative expression of oil red O staining. Measurement of the size of the oil red O adipocytes, demonstrated that L4F-treatment significantly increased the number of small oil red O, ($p < 0.01$), compared to control (untreated adipose cultures). In contrast to L4F, LY294002 decreased oil red O staining. This was reversed by the addition of L-4F (Figure 11D).

DISCUSSION

In this report, we demonstrate that the Apo-A1, mimetic peptide, L-4F, decreased adipogenesis and improved adiposity. This is manifest by a decrease in both SAT and VAT, a decrease in hepatic lipid content and the presence of increased numbers of adipocytes with smaller cell size. MRI and MRS showed that treatment with L-4F resulted in a decrease in visceral fat and improvement in vascular dysfunction as determined by the increased levels of pAMPK, pAKT and phosphorylation of insulin receptors. Thus, L-4F appears capable of reprogramming vascular tissue and adipocytes in a manner that results in the expression of a new phenotype that contains adipocytes of reduced cell size and restored insulin sensitivity. Four observations substantiate this conclusion.

Firstly, the L-4F mediated prevention of visceral and subcutaneous fat accumulation, measured by MRI, is consistent with the observed decrease in hepatic lipid content. The decrease in lipid content is also consistent with the finding that L-4F treatment produced an elevation of the phosphorylation of insulin receptors at multiple sites. The increased phosphorylation of insulin receptors is a response to the increase in pAMPK and pAKT crosstalk and insulin receptor phosphorylation (Figure 9). The decrease in visceral and subcutaneous fat levels was paralleled by an increase in the number of smaller adipocytes which are considered “healthy” insulin sensitive adipocytes (49). Thus, L-4F acts by preventing adipocytes from increasing in size rather than facilitating the death of larger adipocytes which appear to die off as their size increases (50). The action of L-4F can be considered beneficial in that lipid droplets are of smaller

size (Figure 4) and the hepatic lipid content (Figure 7) is reduced in agreement with a previous report (51). Abdominal fat mass is strongly predictive of cardiovascular risk (12, 28, 29, 52), which may be a result of obesity mediated systemic inflammation. Inflammatory cytokines TNF, IL-6 are and IL-1, markedly elevated in the obese rodent and the human (12, 29, 53-55). There is a direct proportionality of the degree of visceral adiposity and the endothelial dysfunction (12, 13, 29, 52).

Secondly, L-4F treatment decreased serum IL-1 β , CB1 receptor and nuclear levels of SREBP-1 levels. The metabolic syndrome and obesity are characterized by increased serum levels of inflammatory cytokines such as IL-1 β , which decrease insulin sensitivity (56, 57). CB1 receptors in mice increase hepatic lipogenic transcription factor SREBP-1 and fatty acid synthesis (21). Therefore, the L-4F mediated decreases in the levels of IL-1 β and CB1 receptors may contribute to the observed increase in insulin sensitivity.

Thirdly, L-4F administration has been shown to increase HO-1 protein levels and adiponectin both in vitro and in vivo. Decreased levels of serum adiponectin are the result of an increase in the levels of ROS and H₂O₂, thereby, contributing to the pathogenesis of insulin resistance (58, 59). Previous studies have shown that increased levels of HO-1 protein caused a marked increase in serum adiponectin levels in Zucker ob rats and ob mice (12, 28, 29). An increase in adiponectin levels is regarded as an indicator of an improvement in the metabolic syndrome which, in turn, leads to increased insulin sensitivity and a subsequent decrease in arterial disease and heart disease (49, 57, 60-63). This

supports the concept that expansion of adipogenesis leads to an increased number of adipocytes of smaller cell size; smaller adipocytes are considered to be healthy, insulin sensitive adipocyte cells that are capable of producing adiponectin (49). While increases in obesity and diabetes are considered risk factors for cardiovascular complications (57), improvement in the diabetic phenotype, including increases in insulin sensitivity and glucose tolerance, may occur through increased pre-adipocyte differentiation and increased adiponectin secretion (49, 64).

Fourthly, increases in HO-1 protein and adiponectin levels have been reported to be associated with an increase in pAKT and pAMPK and an improvement in glucose tolerance. Inhibition of pAKT and pAMPK by LY294002, reversed glucose tolerance and insulin sensitivity (Figure 10A,B). Activated AMPK and PI3K/AKT signaling participates in regulation of cell survival and protects against oxidative stress (22, 65-67). Activation of pAMPK and pAKT, increases phosphorylation of a number of target molecules resulting in an increase in glucose transport and fatty acid oxidation (68, 69). We previously reported that LY294002 inhibition of the AKT pathway prevented increased expression of HO-1 from providing cell protection against ROS (47). Since pAKT and pAMPK act as fuel sensors in the regulation of energy balance at both the cellular and whole body levels, their involvement in the action of L-4F provides an insight into how L-4F may act as an anti-diabetic and anti-obesity agent. This novel effect of L-4F on the HO-1-adiponectin-pAKT-pAMPK functional module i.e., an increase in HO-1, an increase in adiponectin and the subsequent

increase in pAKT and pAMPK, provide a mechanistic basis for L-4F-mediated increases in insulin receptors phosphorylation and vascular protection. Since insulin resistance is an independent risk factor for the development of vascular dysfunction and NO availability (70-72), L-4F-mediated improvement in vascular function, improved glucose tolerance and insulin sensitivity, appears to require an increase in the phosphorylation of insulin receptors.

The increase in pAMPK and pAKT as a result of L-4F treatment may be a direct result of increased adiponectin levels. pAMPK is known to be a downstream signal for adiponectin (73, 74). L-4F-mediated increase in pAKT and pAMPK is essential for restoration of vascular function. Others have suggested that pAMPK can be a therapeutic target for the amelioration of endothelial dysfunction, and of vascular disease (75-77). Induction of the AMPK-AKT system is considered an important metabolic response to attenuate ROS-mediated endothelial dysfunction (75). Thus, there appears a temporal relationship between increased levels of HO expression, adiponectin and pAMPK/pAKT that affords protection against endothelial dysfunction resulting in improved vascular function in the obese diabetic mouse. In addition, the present study is of considerable interest from a clinical and basic science perspective, highlighting the importance of L-4F as a means of reducing adipogenesis. L4F offers potential as a therapeutic means, to address the metabolic derangements associated with obesity, the metabolic syndrome and insulin resistant diabetes.

ACKNOWLEDGEMENTS

This work was supported by NIH grants DK068134, HL55601 and HL34300 (NGA) the Beatrice Renfield Foundation (AK), the CNR Medical Department and Cardiopulmonary Project and the Scuola Sant'Anna. The authors are indebted to Ms Daniele DeMarchi and Dr. Alessandro Pingipore for their valuable help in the acquisition of MR data.

Send reprint requests to: Dr Attallah Kappas, The Rockefeller University, 1230 York Avenue, NY, NY 10021, Tel: 212-327-8494; Dr. Nader G. Abraham, Professor of Pharmacology and Medicine, New York Medical College, Valhalla, NY 10595, E-mail: nader_abraham@nymc.edu

FIGURE LEGENDS

Figure 1: Effect of L-4F on body weight and visceral fat content in lean and ob mice. **A)** Effect of L-4F administration on body appearance; **B)** Examples of subcutaneous and visceral fat and **C)** Dissected fat from lean and ob mice. Representative photographs showing one mouse from each group after 6 weeks of treatment n=8.

Figure 2) Effect of L-4F treatment on Global SAT and VAT as measured by MRI. Global fat was increased in ob mice compared to ob-L-4F-treated mice, * p<0.01, n=3.

Figure 3) Effect of L-4F on gastrocnemius, muscle fibril diameter and muscle weight. **A)** Hematoxylin Eosin staining of gastrocnemius and oil red O staining within myofibril interstitial space in muscle cross section, small arrow indicates extracellular fat deposit and large arrow indicates intracellular fat deposits. A-lean, B-ob fat, C-ob fat L-4F. The mean diameter of myofibril of the lean versus obese p<0.05; **B)** muscle fibril diameter, arrow indicates transverse cut muscle fibers and **C)** muscle weight were measured as described in the methods section. The results are expressed mean \pm SE, n=4. **D)** oil red o muscle fat staining showing increased staining in ob mice and not reduced by L-4F *p<0.005.

Figure 4: A) Haematoxylin-eosin staining of subcutaneous **(A)** and visceral **(B)** fat in ob and L-4F treated ob mice. Bar 50 μm . Quantitative analysis of adipocyte size in subcutaneous fat and visceral fat surrounding the aorta of ob or L4F treated ob mice are displayed. Data are expressed as means \pm S.D. * $P < 0.05$ vs. ob.

Figure 5: A) Immunohistochemistry staining for CB-1 receptor of subcutaneous fat (a-ob and b-ob-L-4F) and visceral fat surrounding aorta (c, obese and d, obese-L-4F) of ob and L-4F treated ob mice. Arrows indicate CB-1 immunoreactivity. Bar.50 μm and **B):** Integrated optical density of CB-1 expression in subcutaneous fat and visceral fat surrounding aorta of ob or L-4F treated ob mice is displayed. Data are expressed as means \pm S.D. * $P < 0.05$ vs. obese mice.

Figure 6: A) Immunohistochemistry staining for HO-1 of subcutaneous fat and visceral fat surrounding aorta of ob or L-4F treated ob mice. Arrows indicate HO-1 immunoreactivity. Bar.50 μm and **B)** Integrated optical density of HO-1 expression in subcutaneous fat and visceral fat surrounding aorta of ob or L-4F treated ob mice. Data are expressed as means \pm S.D. * $P < 0.05$ SAT and VAT.

Figure 7. Effect of L-4F on percentage of fat in the liver of ob mice measured by MRS. Analysis of lipid content and percent of fat increases was calculated as described in the methods section, * $p < 0.01$ vs. obese, $n = 3$.

Figure 8. Effect of L-4F treatment on SREBP-1 measured by Immunohistochemistry in ob and lean mice. A positive SREBP-1 cytoplasmic compartment staining is observed in the kidney of lean (A), ob (B) and ob mice treated with L-4F (C). * $p < 0.04$ ob vs. ob-L-4F, $n = 6$. SREBP-1 increased in nuclear compartments compared to lean. The increase in SREBP-1 was decreased by treatment with L-4F (Magnification X 400).

Figure 9A and B. Effect of L-4F on insulin receptor phosphorylation. **A)** Western blot and densitometry analysis of insulin receptor phosphorylation and actin proteins in liver of lean, ob and ob-treated with L-4F and **B)** Effect of diabetes and L-4F treatment on liver phosphorylation of insulin receptors (upper panel) Tyr 972 and Tyr 1146. Quantitative densitometry evaluation of p-Tyr 972 and Tyr 1146 and actin proteins ratio was determined. Representative Immunoblots are shown, ($n = 5$).

Figure 10 A and B. Effect of HO-1 expression on glucose tolerance and pAMPK and Adiponectin. **A)** Effect of LY294002 (three times/week for three weeks, administered by intraperitoneal injection on glucose tolerance (IPGTT) tests in obese, L-4F-obese, were performed as described in the methods. The

results are expressed mean \pm SE, n=3 and **B)** Western blot of HO-1, adiponectin, pAKT, pAMPK and actin proteins in kidney of ob, ob-treated with L-4F and ob-treated with L-4F and LY294002. Representative Immunoblots are shown, (n= 4).

Figure 11: Effect of LY294002 on L-4F-mediated MSC-derived adipogenesis.

A) Adipogenesis was measured as the relative absorbance of oil red O at day 10 after inducing adipogenesis as described in Methods. Results are mean \pm SE, n=4; *p<0.01 vs. control medium; #p<0.005 vs. high glucose. **B)** Measurement of lipid droplet size. **C)** Scan of lipid size **D)** comparison of the number of small lipids.

REFERENCES

1. Navab, M., G. M. Anantharamaiah, S. T. Reddy, S. Hama, G. Hough, V. R. Grijalva, A. C. Wagner, J. S. Frank, G. Datta, D. Garber, and A. M. Fogelman. 2004. Oral D-4F causes formation of pre-beta high-density lipoprotein and improves high-density lipoprotein-mediated cholesterol efflux and reverse cholesterol transport from macrophages in apolipoprotein E-null mice. *Circulation* **109**: 3215-3220.
2. Navab, M., G. M. Anantharamaiah, S. T. Reddy, B. J. Van Lenten, B. J. Ansell, G. C. Fonarow, K. Vahabzadeh, S. Hama, G. Hough, N. Kamranpour, J. A. Berliner, A. J. Lusis, and A. M. Fogelman. 2004. The oxidation hypothesis of atherogenesis: the role of oxidized phospholipids and HDL. *J. Lipid Res.* **45**: 993-1007.
3. Navab, M., G. M. Anantharamaiah, S. T. Reddy, B. J. Van Lenten, G. Hough, A. Wagner, K. Nakamura, D. W. Garber, G. Datta, J. P. Segrest, S. Hama, and A. M. Fogelman. 2003. Human apolipoprotein AI mimetic peptides for the treatment of atherosclerosis. *Curr. Opin. Investig. Drugs* **4**: 1100-1104.
4. Ou, Z., J. Ou, A. W. Ackerman, K. T. Oldham, and K. A. Pritchard, Jr. 2003. L-4F, an apolipoprotein A-1 mimetic, restores nitric oxide and superoxide anion balance in low-density lipoprotein-treated endothelial cells. *Circulation* **107**: 1520-1524.

5. Ou, J., Z. Ou, D. W. Jones, S. Holzhauer, O. A. Hatoum, A. W. Ackerman, D. W. Weihrauch, D. D. Gutterman, K. Guice, K. T. Oldham, C. A. Hillery, and K. A. Pritchard, Jr. 2003. L-4F, an apolipoprotein A-1 mimetic, dramatically improves vasodilation in hypercholesterolemia and sickle cell disease. *Circulation* **107**: 2337-2341.
6. Kruger, A. L., S. Peterson, S. Turkseven, P. M. Kaminski, F. F. Zhang, S. Quan, M. S. Wolin, and N. G. Abraham. 2005. D-4F induces heme oxygenase-1 and extracellular superoxide dismutase, decreases endothelial cell sloughing, and improves vascular reactivity in rat model of diabetes. *Circulation* **111**: 3126-3134.
7. Peterson, S. J., D. Husney, A. L. Kruger, R. Olszanecki, F. Ricci, L. F. Rodella, A. Stacchiotti, R. Rezzani, J. A. McClung, W. S. Aronow, S. Ikehara, and N. G. Abraham. 2007. Long-term treatment with the apolipoprotein A1 mimetic Peptide increases antioxidants and vascular repair in type I diabetic rats. *J Pharmacol. Exp. Ther.* **322**: 514-520.
8. Morino, K., S. Neschen, S. Bilz, S. Sono, D. Tsigotis, R. M. Reznick, I. Moore, Y. Nagai, V. Samuel, D. Sebastian, M. White, W. Philbrick, and G. I. Shulman. 2008. Muscle specific IRS-1 Ser->Ala transgenic mice are protected from fat-induced insulin resistance in skeletal muscle. *Diabetes*.
9. Danial, N. N., L. D. Walensky, C. Y. Zhang, C. S. Choi, J. K. Fisher, A. J. Molina, S. R. Datta, K. L. Pitter, G. H. Bird, J. D. Wikstrom, J. T. Deeney, K. Robertson, J. Morash, A. Kulkarni, S. Neschen, S. Kim, M. E.

- Greenberg, B. E. Corkey, O. S. Shirihai, G. I. Shulman, B. B. Lowell, and S. J. Korsmeyer. 2008. Dual role of proapoptotic BAD in insulin secretion and beta cell survival. *Nat. Med.* **14**: 144-153.
10. Wellen, K. E. and G. S. Hotamisligil. 2003. Obesity-induced inflammatory changes in adipose tissue. *J Clin. Invest* **112**: 1785-1788.
11. Weisberg, S. P., D. Hunter, R. Huber, J. Lemieux, S. Slaymaker, K. Vaddi, I. Charo, R. L. Leibel, and A. W. Ferrante, Jr. 2006. CCR2 modulates inflammatory and metabolic effects of high-fat feeding. *J Clin. Invest* **116**: 115-124.
12. Li, M., D. H. Kim, P. L. Tsenovoy, S. J. Peterson, R. Rezzani, L. F. Rodella, W. S. Aronow, S. Ikehara, and N. G. Abraham. 2008. Treatment of obese diabetic mice with a heme oxygenase inducer reduces visceral and subcutaneous adiposity, increases adiponectin levels, and improves insulin sensitivity and glucose tolerance. *Diabetes* **57**: 1526-1535.
13. Eckel, R. H., D. A. York, S. Rossner, V. Hubbard, I. Caterson, S. T. St Jeor, L. L. Hayman, R. M. Mullis, and S. N. Blair. 2004. Prevention Conference VII: Obesity, a worldwide epidemic related to heart disease and stroke: executive summary. *Circulation* **110**: 2968-2975.
14. Tounian, P., Y. Aggoun, B. Dubern, V. Varille, B. Guy-Grand, D. Sidi, J. P. Girardet, and D. Bonnet. 2001. Presence of increased stiffness of the

- common carotid artery and endothelial dysfunction in severely obese children: a prospective study. *Lancet* **358**: 1400-1404.
15. Kruger, A. L., S. J. Peterson, M. L. Schwartzman, H. Fusco, J. A. McClung, M. Weiss, S. Shenouda, A. I. Goodman, M. S. Goligorsky, A. Kappas, and N. G. Abraham. 2006. Up-regulation of heme oxygenase provides vascular protection in an animal model of diabetes through its antioxidant and antiapoptotic effects. *J Pharmacol. Exp. Ther.* **319**: 1144-1152.
 16. Abraham NG and A. Kappas. 2008. Pharmacological and clinical aspects of heme oxygenase. *Pharmacol. Rev.* **60**: 79-127.
 17. Steinberg, H. O., H. Chaker, R. Leaming, A. Johnson, G. Brechtel, and A. D. Baron. 1996. Obesity/insulin resistance is associated with endothelial dysfunction. Implications for the syndrome of insulin resistance. *J. Clin. Invest* **97**: 2601-2610.
 18. Yudkin, J. S., M. Kumari, S. E. Humphries, and V. Mohamed-Ali. 2000. Inflammation, obesity, stress and coronary heart disease: is interleukin-6 the link? *Atherosclerosis* **148**: 209-214.
 19. Zhang, F., J. I. Kaide, L. Yang, H. Jiang, S. Quan, R. Kemp, W. Gong, M. Balazy, N. G. Abraham, and A. Nasjletti. 2004. CO modulates pulmonary vascular response to acute hypoxia: relation to endothelin. *Am. J Physiol Heart Circ. Physiol* **286**: H137-H144.

20. Porstmann, T., B. Griffiths, Y. L. Chung, O. Delpuech, J. R. Griffiths, J. Downward, and A. Schulze. 2005. PKB/Akt induces transcription of enzymes involved in cholesterol and fatty acid biosynthesis via activation of SREBP. *Oncogene* **24**: 6465-6481.
21. Osei-Hyiaman, D., M. DePetrillo, P. Pacher, J. Liu, S. Radaeva, S. Batkai, J. Harvey-White, K. Mackie, L. Offertaler, L. Wang, and G. Kunos. 2005. Endocannabinoid activation at hepatic CB1 receptors stimulates fatty acid synthesis and contributes to diet-induced obesity. *J Clin. Invest* **115**: 1298-1305.
22. Di Noia, M. A., D. S. Van, F. Palmieri, L. M. Yang, S. Quan, A. I. Goodman, and N. G. Abraham. 2006. Heme oxygenase-1 enhances renal mitochondrial transport carriers and cytochrome C oxidase activity in experimental diabetes. *J Biol. Chem.* **281**: 15687-15693.
23. Li, M., S. Peterson, D. Husney, M. Inaba, K. Guo, E. Terada, T. Morita, K. Patil, A. Kappas, S. Ikehara, and N. G. Abraham. 2007. Interdiction of the diabetic state in NOD mice by sustained induction of heme oxygenase: possible role of carbon monoxide and bilirubin. *Antioxid. Redox Signal.* **9**: 855-863.
24. Zhang, Y., T. S. Lee, E. M. Kolb, K. Sun, X. Lu, F. M. Sladek, G. S. Kassab, T. Garland, Jr., and J. Y. Shyy. 2006. AMP-activated protein kinase is involved in endothelial NO synthase activation in response to shear stress. *Arterioscler. Thromb. Vasc. Biol.* **26**: 1281-1287.

25. Fleming, I., C. Schulz, B. Fichtlscherer, B. E. Kemp, B. Fisslthaler, and R. Busse. 2003. AMP-activated protein kinase (AMPK) regulates the insulin-induced activation of the nitric oxide synthase in human platelets. *Thromb. Haemost.* **90**: 863-871.
26. Reihill, J. A., M. A. Ewart, D. G. Hardie, and I. P. Salt. 2007. AMP-activated protein kinase mediates VEGF-stimulated endothelial NO production. *Biochem. Biophys. Res. Commun.* **354**: 1084-1088.
27. Fleming, I., B. Fisslthaler, M. Dixit, and R. Busse. 2005. Role of PECAM-1 in the shear-stress-induced activation of Akt and the endothelial nitric oxide synthase (eNOS) in endothelial cells. *J. Cell Sci.* **118**: 4103-4111.
28. Kim, D. H., A. P. Burgess, M. Li, P. L. Tsenovoy, F. Addabbo, J. A. McClung, N. Puri, and N. G. Abraham. 2008. Heme oxygenase-mediated increases in adiponectin decrease fat content and inflammatory cytokines, tumor necrosis factor-alpha and interleukin-6 in Zucker rats and reduce adipogenesis in human mesenchymal stem cells. *J Pharmacol. Exp. Ther.* **325**: 833-40.
29. Peterson, S. J., G. Drummond, K. D. Hyun, M. Li, A. L. Kruger, S. Ikehara, and N. G. Abraham. 2008. L-4F treatment reduces adiposity, increases adiponectin levels and improves insulin sensitivity in obese mice. *J Lipid Res* **49**: 1658-1669.

30. Sun, J. F., T. Phung, I. Shiojima, T. Felske, J. N. Upalakin, D. Feng, T. Kornaga, T. Dor, A. M. Dvorak, K. Walsh, and L. E. Benjamin. 2005. Microvascular patterning is controlled by fine-tuning the Akt signal. *Proc. Natl. Acad. Sci. U. S. A* **102**: 128-133.
31. Sambuceti, G., S. Morbelli, L. Vanella, C. Kusmic, C. Marini, M. Massollo, C. Augeri, M. Corselli, C. Gherzi, B. Chiavarina, L. Rodella, A. L'Abbate, G. Drummond, N. G. Abraham, and F. Frassoni. 2009. Diabetes impairs the vascular recruitment of normal stem cells by oxidant damage reversed by increases in pAMPK, heme oxygenase-1 and adiponectin. *Stem Cells* **[Ahead of Pub]**.
32. Kovacic, S., C. L. Soltys, A. J. Barr, I. Shiojima, K. Walsh, and J. R. Dyck. 2003. Akt activity negatively regulates phosphorylation of AMP-activated protein kinase in the heart. *J. Biol. Chem.* **278**: 39422-39427.
33. Kronke, G., A. Kadl, E. Ikonomu, S. Bluml, A. Furnkranz, I. J. Sarembock, V. N. Bochkov, M. Exner, B. R. Binder, and N. Leitinger. 2007. Expression of heme oxygenase-1 in human vascular cells is regulated by peroxisome proliferator-activated receptors. *Arterioscler. Thromb. Vasc. Biol.* **27**: 1276-1282.
34. L'Abbate, A., D. Neglia, C. Vecoli, M. Novelli, V. Ottaviano, S. Baldi, R. Barsacchi, A. Paolicchi, P. Masiello, G. Drummond, J. McClung, and N. Abraham. 2007. Beneficial effect of heme oxygenase-1 expression in

- myocardial ischemia-reperfusion increases adiponectin in mildly diabetic rats. *Am. J. Physiol. Heart Circ. Physiol.* **293**: H3532-H3541.
35. Heinecke, J. W. 2006. Lipoprotein oxidation in cardiovascular disease: chief culprit or innocent bystander? *J. Exp. Med.* **203**: 813-816.
36. Oberle, S., A. Abate, N. Grosser, A. Hemmerle, H. J. Vreman, P. A. Dennerly, H. T. Schneider, D. Stalleicken, and H. Schroder. 2003. Endothelial protection by pentaerythryl trinitrate: bilirubin and carbon monoxide as possible mediators. *Exp. Biol. Med. (Maywood.)* **228**: 529-534.
37. Grosser, N., K. Erdmann, A. Hemmerle, G. Berndt, U. Hinkelmann, G. Smith, and H. Schroder. 2004. Rosuvastatin upregulates the antioxidant defense protein heme oxygenase-1. *Biochem. Biophys. Res. Commun.* **325**: 871-876.
38. Grosser, N., A. Hemmerle, G. Berndt, K. Erdmann, U. Hinkelmann, S. Schurgerc, N. Wijayanti, S. Immenschuh, and H. Schroder. 2004. The antioxidant defense protein heme oxygenase 1 is a novel target for statins in endothelial cells. *Free Radic. Biol. Med.* **37**: 2064-2071.
39. Lee, T. S., C. C. Chang, Y. Zhu, and J. Y. Shyy. 2004. Simvastatin induces heme oxygenase-1: a novel mechanism of vessel protection. *Circulation* **110**: 1296-1302.

40. Navab, M., G. M. Anantharamaiah, S. Hama, D. W. Garber, M. Chaddha, G. Hough, R. Lallone, and A. M. Fogelman. 2002. Oral administration of an Apo A-I mimetic Peptide synthesized from D-amino acids dramatically reduces atherosclerosis in mice independent of plasma cholesterol. *Circulation* **105**: 290-292.
41. Hu, L., J. Hofmann, and R. B. Jaffe. 2005. Phosphatidylinositol 3-kinase mediates angiogenesis and vascular permeability associated with ovarian carcinoma. *Clin. Cancer Res* **11**: 8208-8212.
42. Positano, V., A. Gastaldelli, A. M. Sironi, M. F. Santarelli, M. Lombardi, and L. Landini. 2004. An accurate and robust method for unsupervised assessment of abdominal fat by MRI. *J Magn Reson. Imaging* **20**: 684-689.
43. Demerath, E. W., K. J. Ritter, W. A. Couch, N. L. Rogers, G. M. Moreno, A. Choh, M. Lee, K. Remsberg, S. A. Czerwinski, W. C. Chumlea, R. M. Siervogel, and B. Towne. 2007. Validity of a new automated software program for visceral adipose tissue estimation. *Int. J Obes. (Lond)* **31**: 285-291.
44. Bonekamp, S., P. Ghosh, S. Crawford, S. F. Solga, A. Horska, F. L. Brancati, A. M. Diehl, S. Smith, and J. M. Clark. 2008. Quantitative comparison and evaluation of software packages for assessment of abdominal adipose tissue distribution by magnetic resonance imaging. *Int. J Obes. (Lond)* **32**: 100-111.

45. Novikoff, A. B., P. M. Novikoff, O. M. Rosen, and C. S. Rubin. 1980. Organelle relationships in cultured 3T3-L1 preadipocytes. *J Cell Biol.* **87**: 180-196.
46. Tondreau, T., N. Meuleman, A. Delforge, M. Dejeneffe, R. Leroy, M. Massy, C. Mortier, D. Bron, and L. Lagneaux. 2005. Mesenchymal stem cells derived from CD133-positive cells in mobilized peripheral blood and cord blood: proliferation, Oct4 expression, and plasticity. *Stem Cells* **23**: 1105-1112.
47. Salinas, M., R. Diaz, N. G. Abraham, C. M. Ruiz De Galarreta, and A. Cuadrado. 2003. Nerve growth factor protects against 6-hydroxydopamine-induced oxidative stress by increasing expression of heme oxygenase-1 in a phosphatidylinositol 3-kinase-dependent manner. *J Biol. Chem.* **278**: 13898-13904.
48. Lee, R. H., B. Kim, I. Choi, H. Kim, H. S. Choi, K. Suh, Y. C. Bae, and J. S. Jung. 2004. Characterization and expression analysis of mesenchymal stem cells from human bone marrow and adipose tissue. *Cell Physiol Biochem.* **14**: 311-324.
49. Kim, J. Y., W. E. van de, M. Laplante, A. Azzara, M. E. Trujillo, S. M. Hofmann, T. Schraw, J. L. Durand, H. Li, G. Li, L. A. Jelicks, M. F. Mehler, D. Y. Hui, Y. Deshaies, G. I. Shulman, G. J. Schwartz, and P. E. Scherer. 2007. Obesity-associated improvements in metabolic profile through expansion of adipose tissue. *J Clin. Invest* **117**: 2621-2637.

50. Kim, J. Y., W. E. van de, M. Laplante, A. Azzara, M. E. Trujillo, S. M. Hofmann, T. Schraw, J. L. Durand, H. Li, G. Li, L. A. Jelicks, M. F. Mehler, D. Y. Hui, Y. Deshaies, G. I. Shulman, G. J. Schwartz, and P. E. Scherer. 2007. Obesity-associated improvements in metabolic profile through expansion of adipose tissue. *J. Clin. Invest* **117**: 2621-2637.
51. Basu, R., U. B. Pajvani, R. A. Rizza, and P. E. Scherer. 2007. Selective downregulation of the high molecular weight form of adiponectin in hyperinsulinemia and in type 2 diabetes: differential regulation from nondiabetic subjects. *Diabetes* **56**: 2174-2177.
52. Williams, I. L., P. J. Chowienczyk, S. B. Wheatcroft, A. Patel, R. Sherwood, A. Momin, A. M. Shah, and M. T. Kearney. 2006. Effect of fat distribution on endothelial-dependent and endothelial-independent vasodilatation in healthy humans. *Diabetes Obes. Metab* **8**: 296-301.
53. Bastard, J. P., M. Maachi, J. T. Van Nhieu, C. Jardel, E. Bruckert, A. Grimaldi, J. J. Robert, J. Capeau, and B. Hainque. 2002. Adipose tissue IL-6 content correlates with resistance to insulin activation of glucose uptake both in vivo and in vitro. *J. Clin. Endocrinol. Metab* **87**: 2084-2089.
54. Maachi, M., L. Pieroni, E. Bruckert, C. Jardel, S. Fellahi, B. Hainque, J. Capeau, and J. P. Bastard. 2004. Systemic low-grade inflammation is related to both circulating and adipose tissue TNFalpha, leptin and IL-6 levels in obese women. *Int. J. Obes. Relat Metab Disord*. **28**: 993-997.

55. Hingorani, A. D., J. Cross, R. K. Kharbanda, M. J. Mullen, K. Bhagat, M. Taylor, A. E. Donald, M. Palacios, G. E. Griffin, J. E. Deanfield, R. J. MacAllister, and P. Vallance. 2000. Acute systemic inflammation impairs endothelium-dependent dilatation in humans. *Circulation* **102**: 994-999.
56. Muse, E. D., T. K. Lam, P. E. Scherer, and L. Rossetti. 2007. Hypothalamic resistin induces hepatic insulin resistance. *J Clin. Invest* **117**: 1670-1678.
57. Lazar, M. A. 2005. How obesity causes diabetes: not a tall tale. *Science* **307**: 373-375.
58. Kondo, H., I. Shimomura, Y. Matsukawa, M. Kumada, M. Takahashi, M. Matsuda, N. Ouchi, S. Kihara, T. Kawamoto, S. Sumitsuji, T. Funahashi, and Y. Matsuzawa. 2002. Association of adiponectin mutation with type 2 diabetes: a candidate gene for the insulin resistance syndrome. *Diabetes* **51**: 2325-2328.
59. Fasshauer, M., J. Klein, S. Neumann, M. Eszlinger, and R. Paschke. 2001. Adiponectin gene expression is inhibited by beta-adrenergic stimulation via protein kinase A in 3T3-L1 adipocytes. *FEBS Lett* **507**: 142-146.
60. Bahia, L., L. G. Aguiar, N. Villela, D. Bottino, A. F. Godoy-Matos, B. Geloneze, M. Tambascia, and E. Bouskela. 2006. Relationship between adipokines, inflammation, and vascular reactivity in lean controls and obese subjects with metabolic syndrome. *Clinics*. **61**: 433-440.

61. Han, S. H., M. J. Quon, J. A. Kim, and K. K. Koh. 2007. Adiponectin and cardiovascular disease: response to therapeutic interventions. *J Am. Coll. Cardiol.* **49**: 531-538.
62. Fontana, L., J. C. Eagon, M. E. Trujillo, P. E. Scherer, and S. Klein. 2007. Visceral fat adipokine secretion is associated with systemic inflammation in obese humans. *Diabetes* **56**: 1010-1013.
63. Iwashima, Y., T. Horio, Y. Suzuki, S. Kihara, H. Rakugi, K. Kangawa, T. Funahashi, T. Ogihara, and Y. Kawano. 2006. Adiponectin and inflammatory markers in peripheral arterial occlusive disease. *Atherosclerosis* **188**: 384-390.
64. Yamauchi, T., Y. Nio, T. Maki, M. Kobayashi, T. Takazawa, M. Iwabuchi, M. Okada-Iwabuchi, S. Kawamoto, N. Kubota, T. Kubota, Y. Ito, J. Kamon, A. Tsuchida, K. Kumagai, H. Kozono, Y. Hada, H. Ogata, K. Tokuyama, M. Tsunoda, T. Ide, K. Murakami, M. Awazawa, I. Takamoto, P. Froguel, K. Hara, K. Tobe, R. Nagai, K. Ueki, and T. Kadowaki. 2007. Targeted disruption of AdipoR1 and AdipoR2 causes abrogation of adiponectin binding and metabolic actions. *Nat. Med.* **13**: 332-339.
65. Hardie, D. G. 2003. Minireview: the AMP-activated protein kinase cascade: the key sensor of cellular energy status. *Endocrinology* **144**: 5179-5183.

66. Skurk, C., H. Maatz, H. S. Kim, J. Yang, M. R. Abid, W. C. Aird, and K. Walsh. 2004. The Akt-regulated forkhead transcription factor FOXO3a controls endothelial cell viability through modulation of the caspase-8 inhibitor FLIP. *J Biol. Chem* **279**: 1513-1525.
67. Hardie, D. G. 2007. AMP-activated protein kinase as a drug target. *Annu. Rev. Pharmacol. Toxicol.* **47**: 185-210.
68. Kurth-Kraczek, E. J., M. F. Hirshman, L. J. Goodyear, and W. W. Winder. 1999. 5' AMP-activated protein kinase activation causes GLUT4 translocation in skeletal muscle. *Diabetes* **48**: 1667-1671.
69. Stoppani, J., A. L. Hildebrandt, K. Sakamoto, D. Cameron-Smith, L. J. Goodyear, and P. D. Neuffer. 2002. AMP-activated protein kinase activates transcription of the UCP3 and HKII genes in rat skeletal muscle. *Am J Physiol Endocrinol. Metab* **283**: E1239-E1248.
70. Duncan, E., P. Crossey, S. Walker, N. Anilkumar, L. Poston, G. Douglas, V. Ezzat, S. Wheatcroft, A. M. Shah, and M. Kearney. 2008. The effect of endothelium specific insulin resistance on endothelial function in vivo. *Diabetes*.
71. Kawakami, A., M. Osaka, M. Tani, H. Azuma, F. M. Sacks, K. Shimokado, and M. Yoshida. 2008. Apolipoprotein CIII links hyperlipidemia with vascular endothelial cell dysfunction. *Circulation* **118**: 731-742.

72. Kearney, M. T., E. R. Duncan, M. Kahn, and S. B. Wheatcroft. 2008. Insulin resistance and endothelial cell dysfunction: studies in mammalian models. *Exp. Physiol* **93**: 158-163.
73. Ouchi, N., H. Kobayashi, S. Kihara, M. Kumada, K. Sato, T. Inoue, T. Funahashi, and K. Walsh. 2004. Adiponectin stimulates angiogenesis by promoting cross-talk between AMP-activated protein kinase and Akt signaling in endothelial cells. *J Biol. Chem.* **279**: 1304-1309.
74. Ouchi, N., R. Shibata, and K. Walsh. 2006. Cardioprotection by adiponectin. *Trends Cardiovasc. Med.* **16**: 141-146.
75. Schulz, E., J. Dopheide, S. Schuhmacher, S. R. Thomas, K. Chen, A. Daiber, P. Wenzel, T. Munzel, and J. F. Keane, Jr. 2008. Suppression of the JNK pathway by induction of a metabolic stress response prevents vascular injury and dysfunction. *Circulation* **118**: 1347-1357.
76. Chen, K., M. T. Kirber, H. Xiao, Y. Yang, and J. F. Keane, Jr. 2008. Regulation of ROS signal transduction by NADPH oxidase 4 localization. *J. Cell Biol.* **181**: 1129-1139.
77. Murabito, J. M., M. J. Keyes, C. Y. Guo, J. F. Keane, Jr., R. S. Vasan, R. B. D'Agostino, Sr., and E. J. Benjamin. 2008. Cross-sectional relations of multiple inflammatory biomarkers to peripheral arterial disease: The Framingham Offspring Study. *Atherosclerosis*.

Fig 1

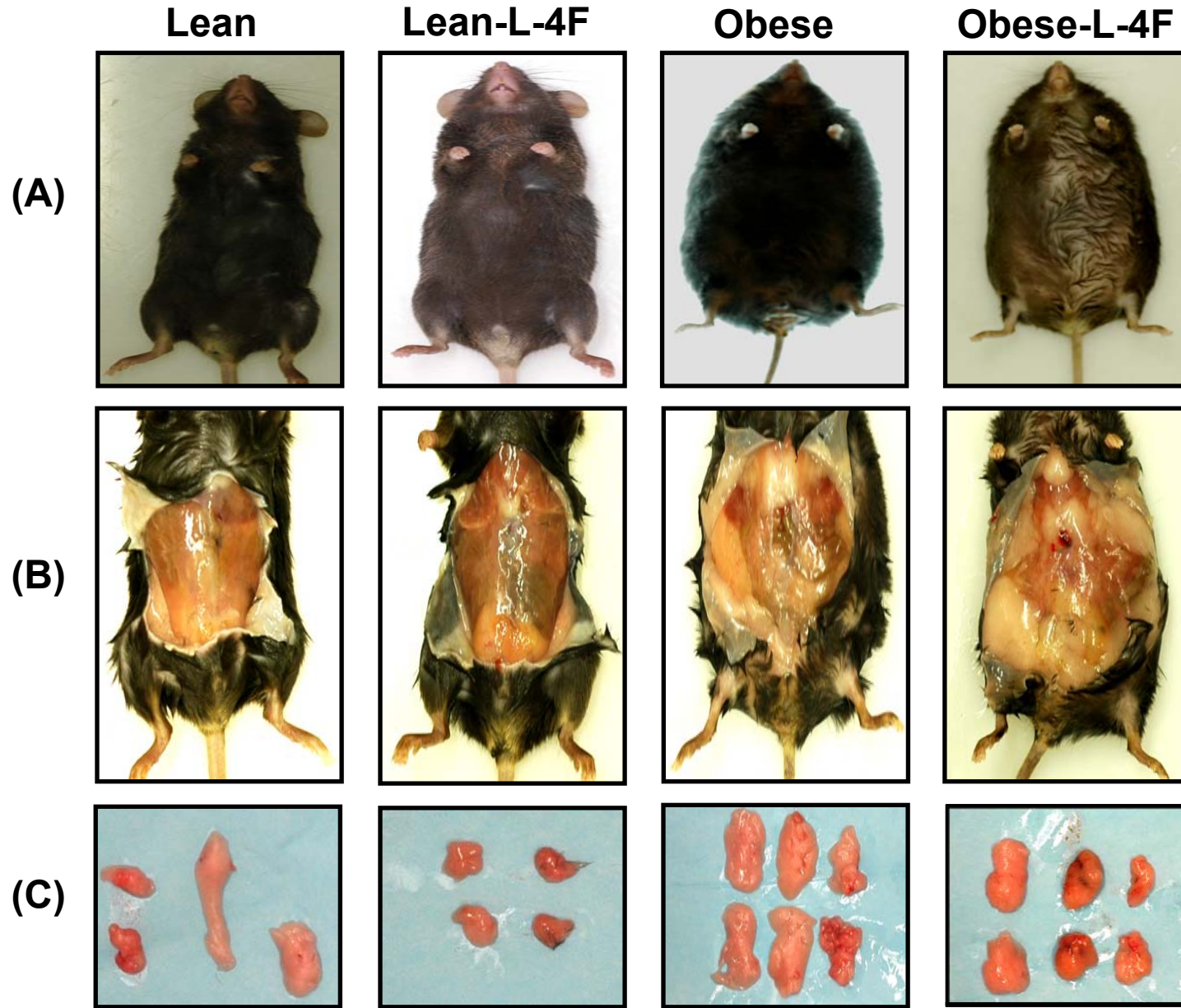


Fig 2

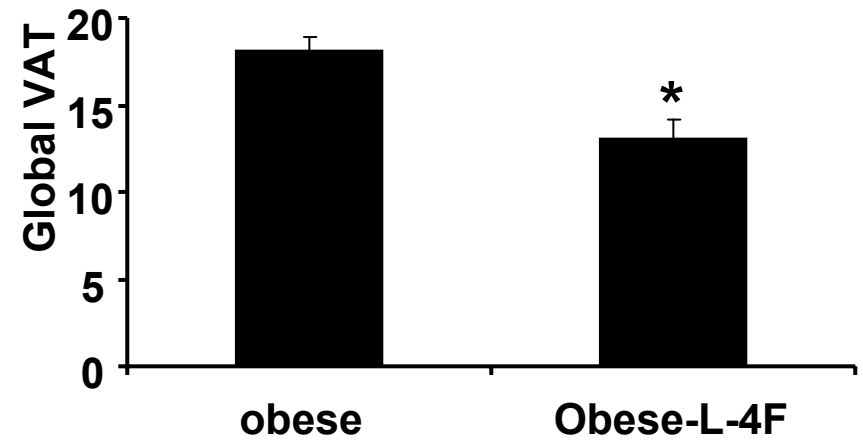
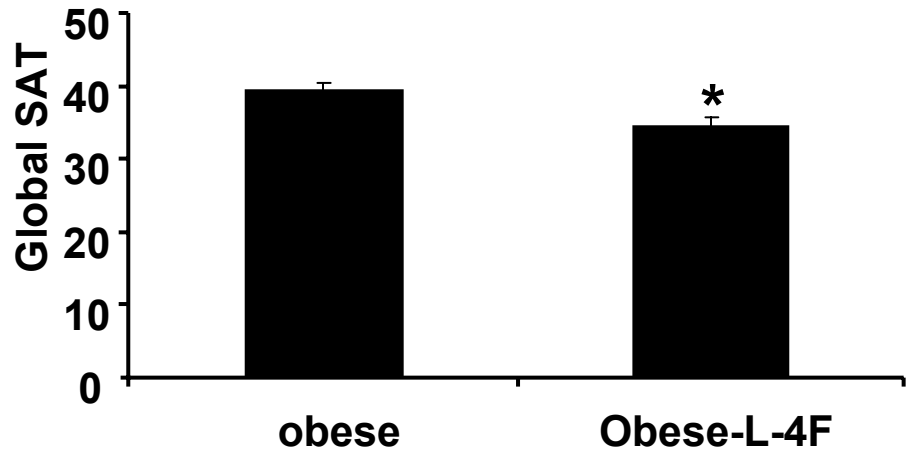
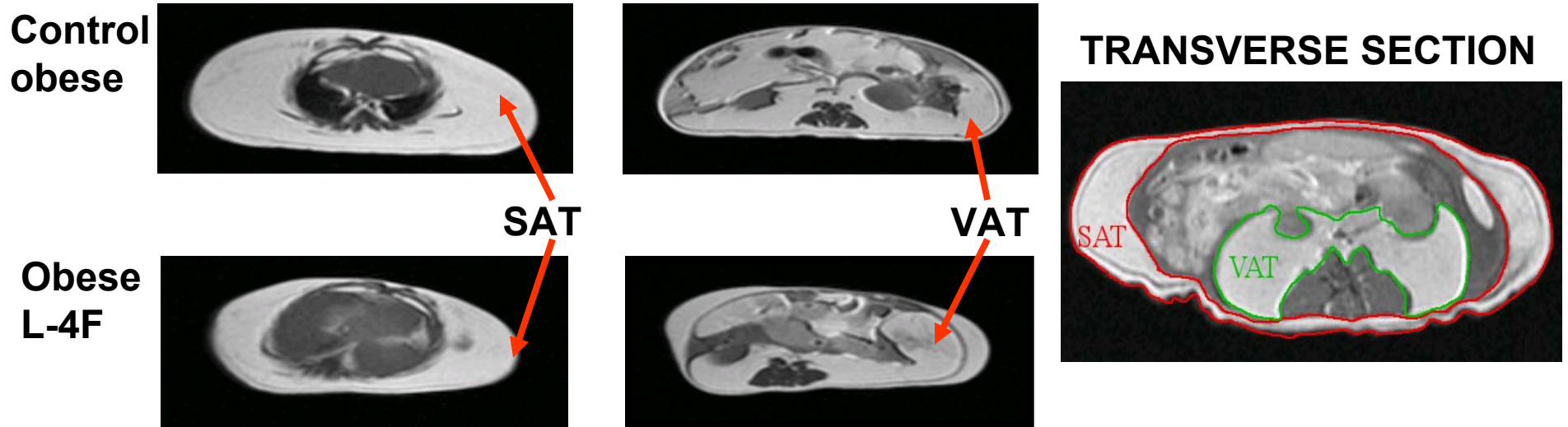


Fig 3

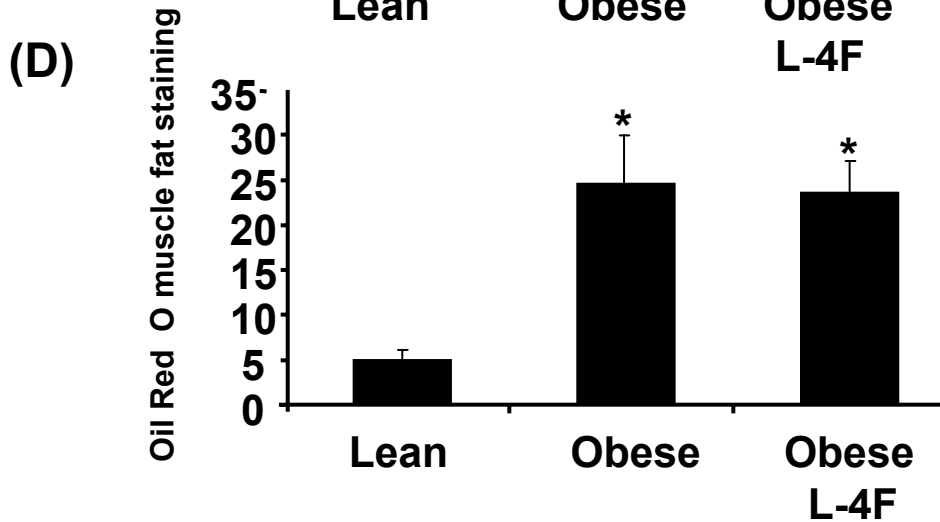
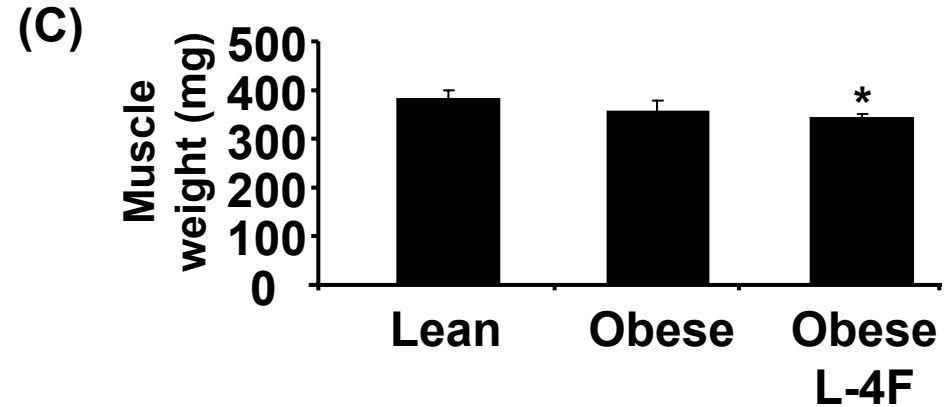
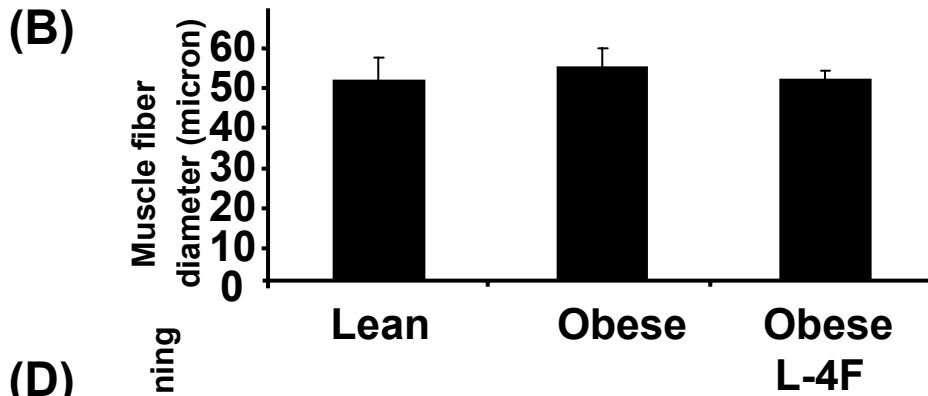
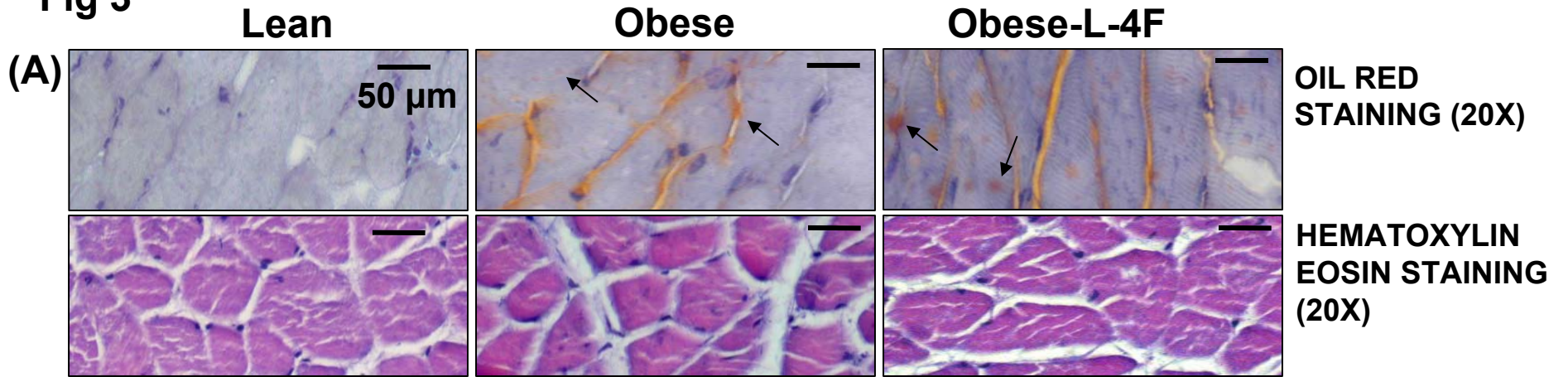


Fig 4 Adipocyte size of Subcutaneous and Visceral Fat

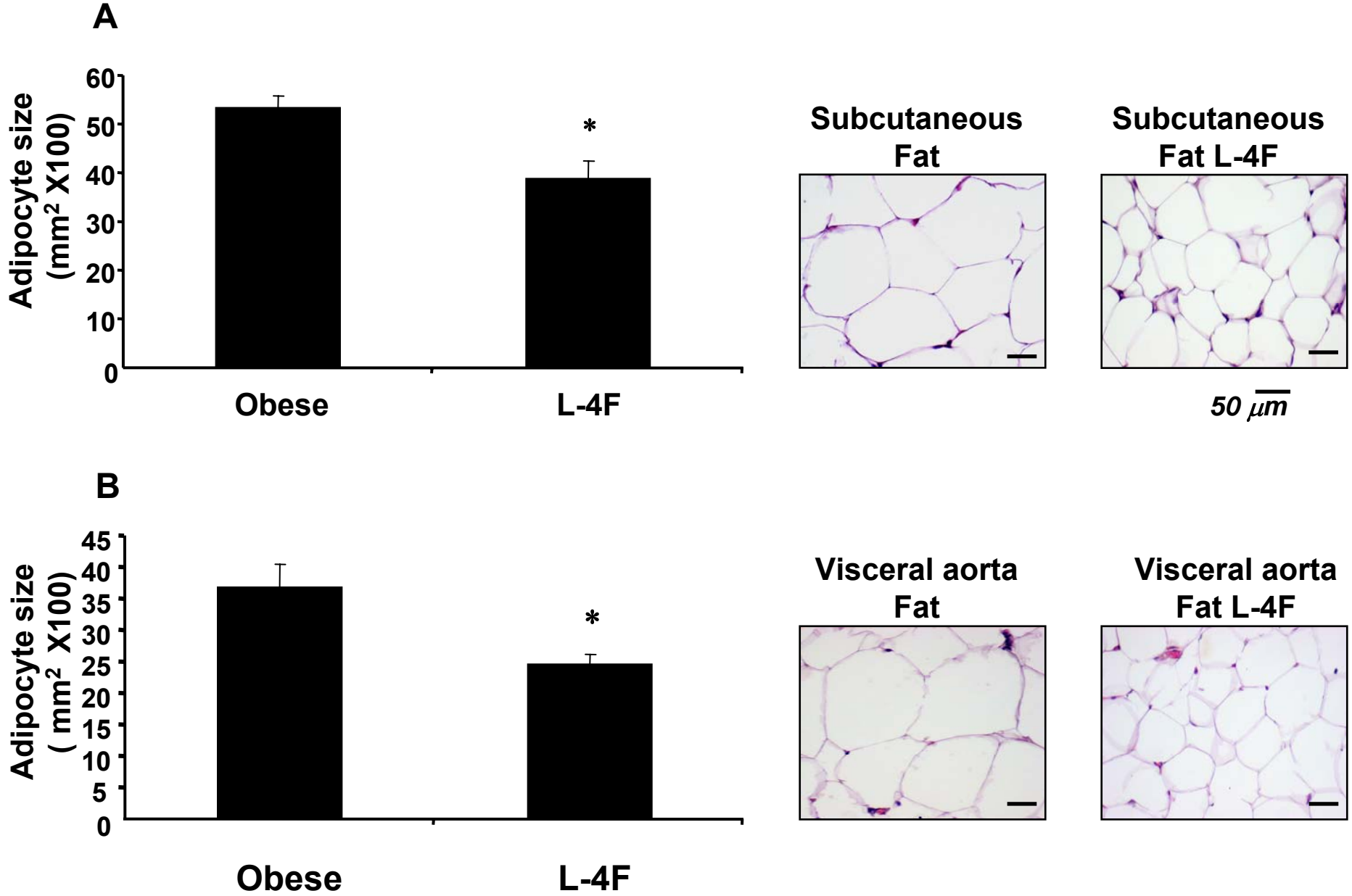


Fig 5

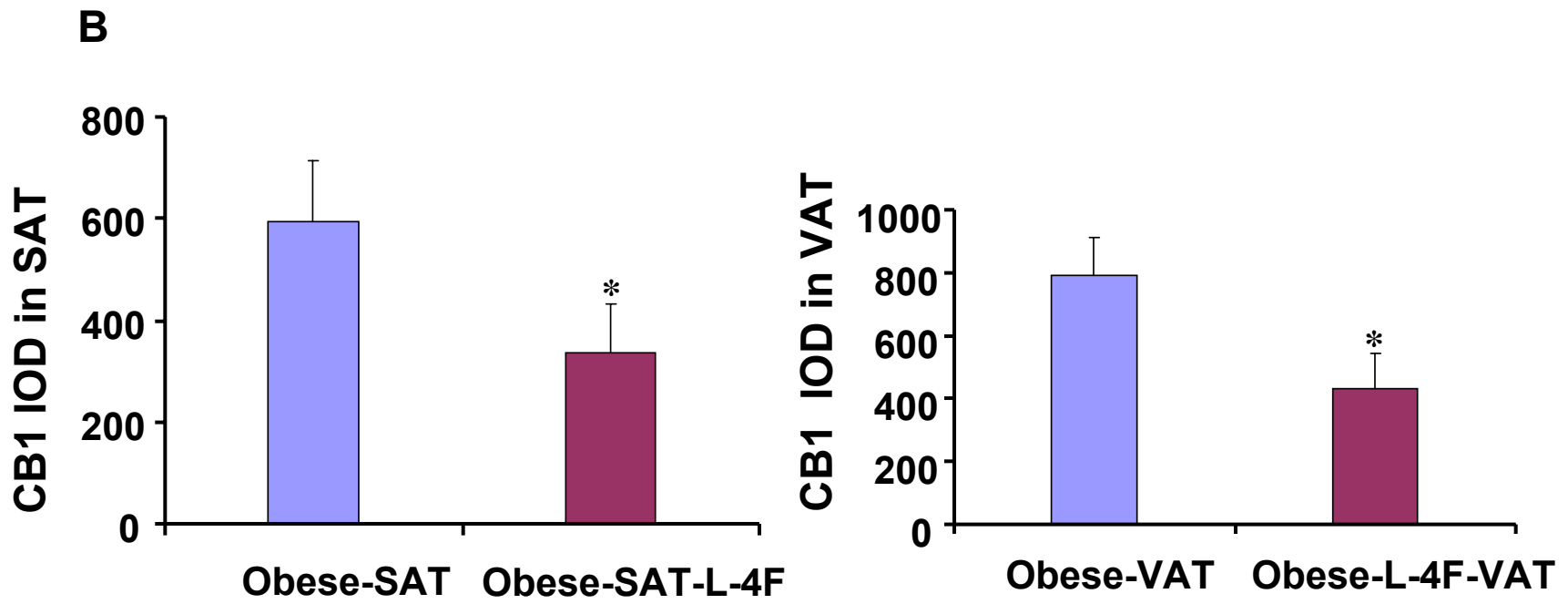
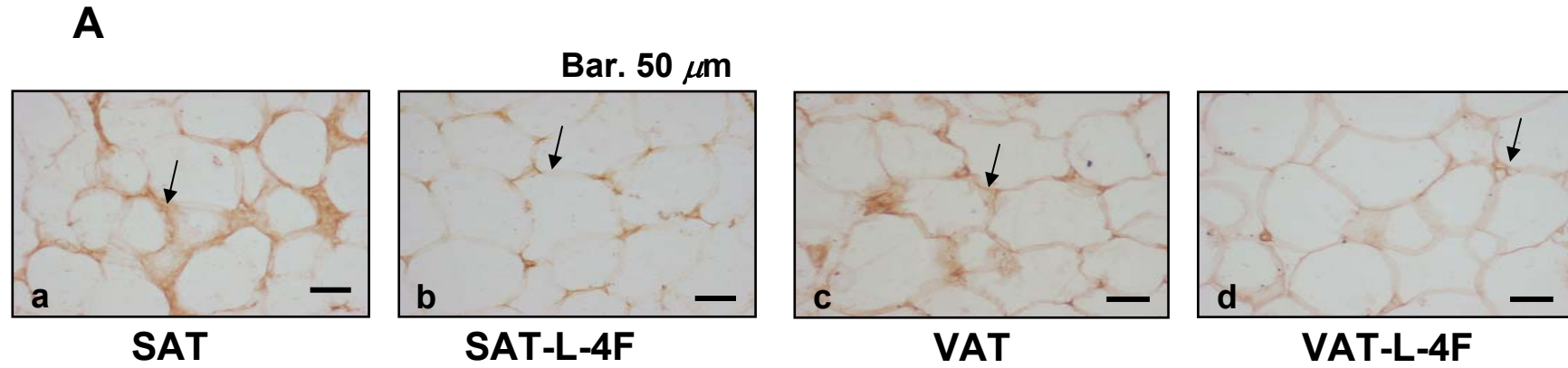
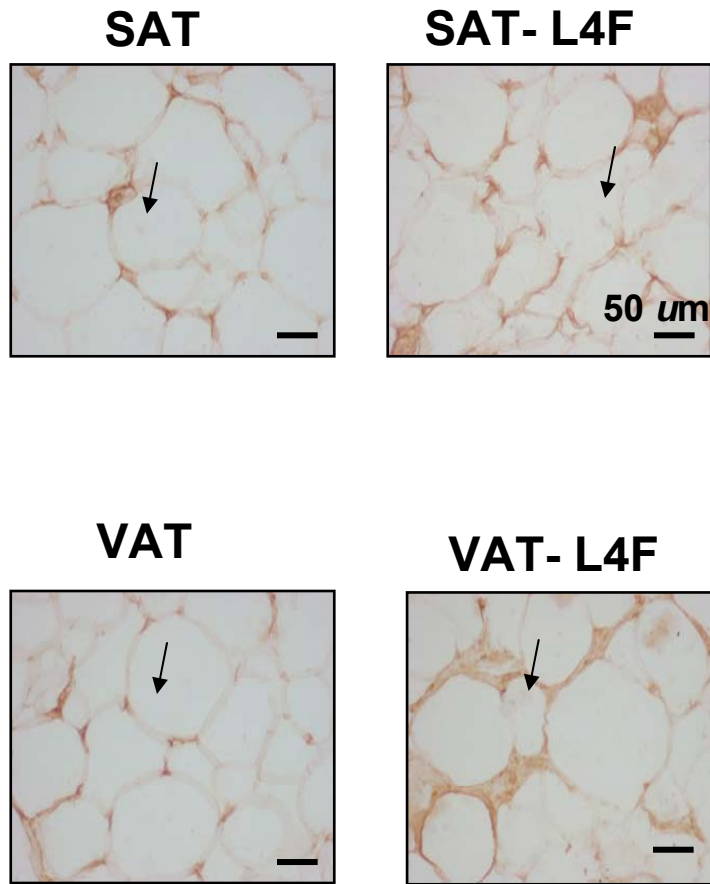


Fig 6

A



B

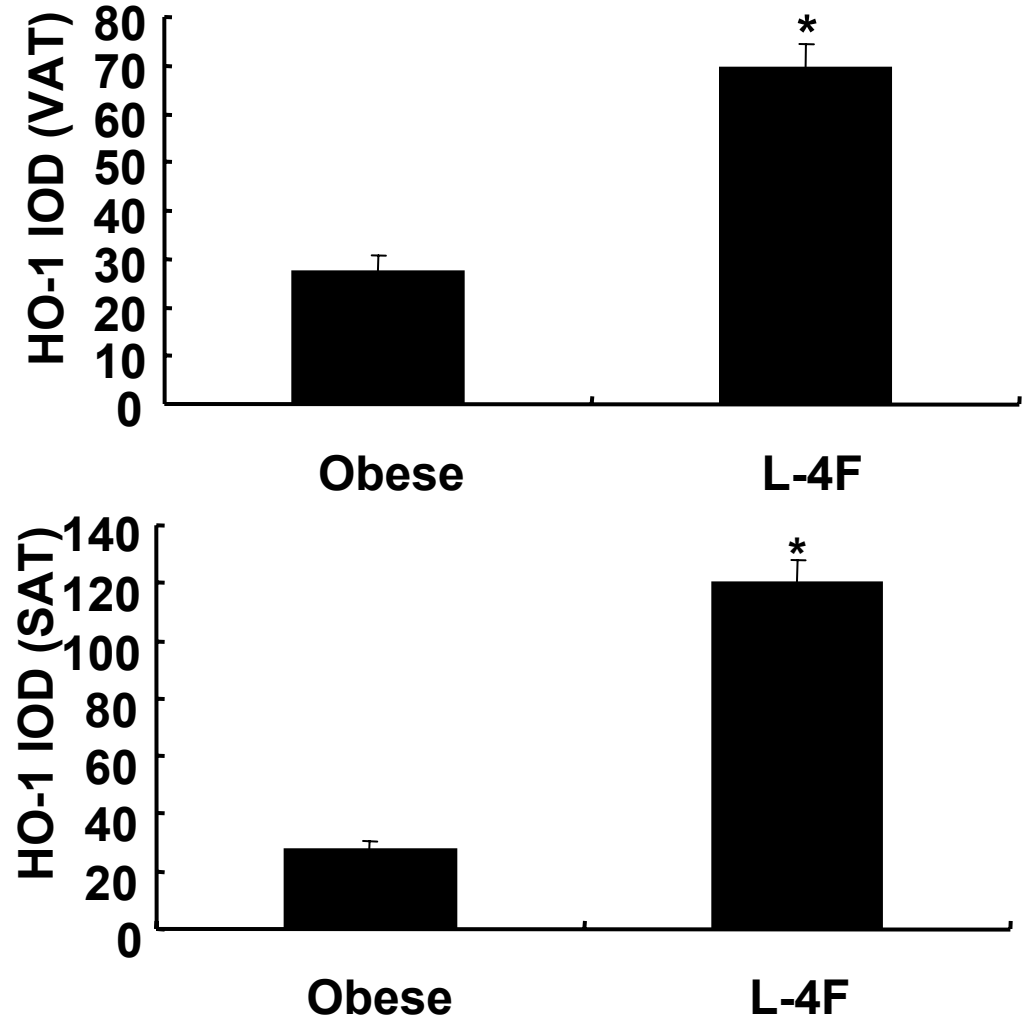


Fig 7

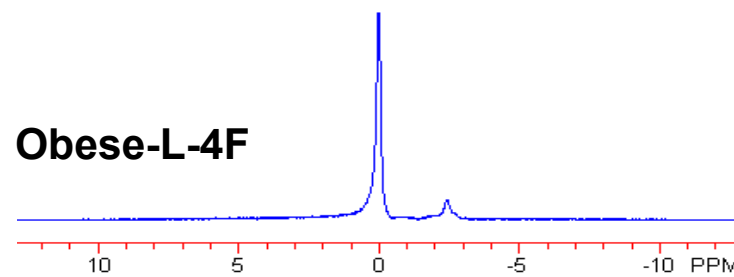
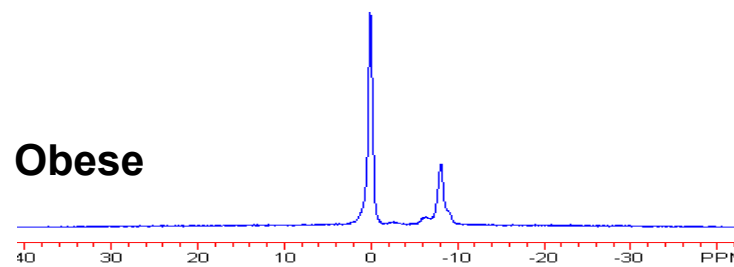
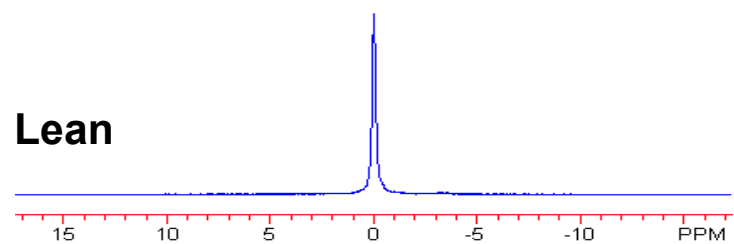
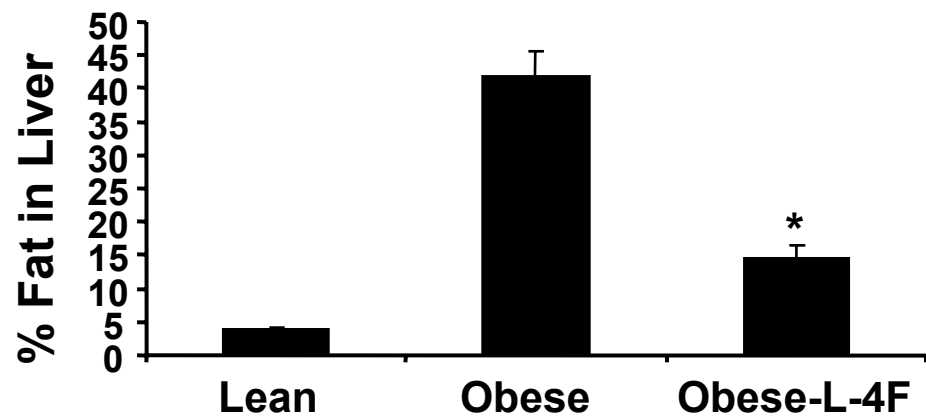


Fig 8

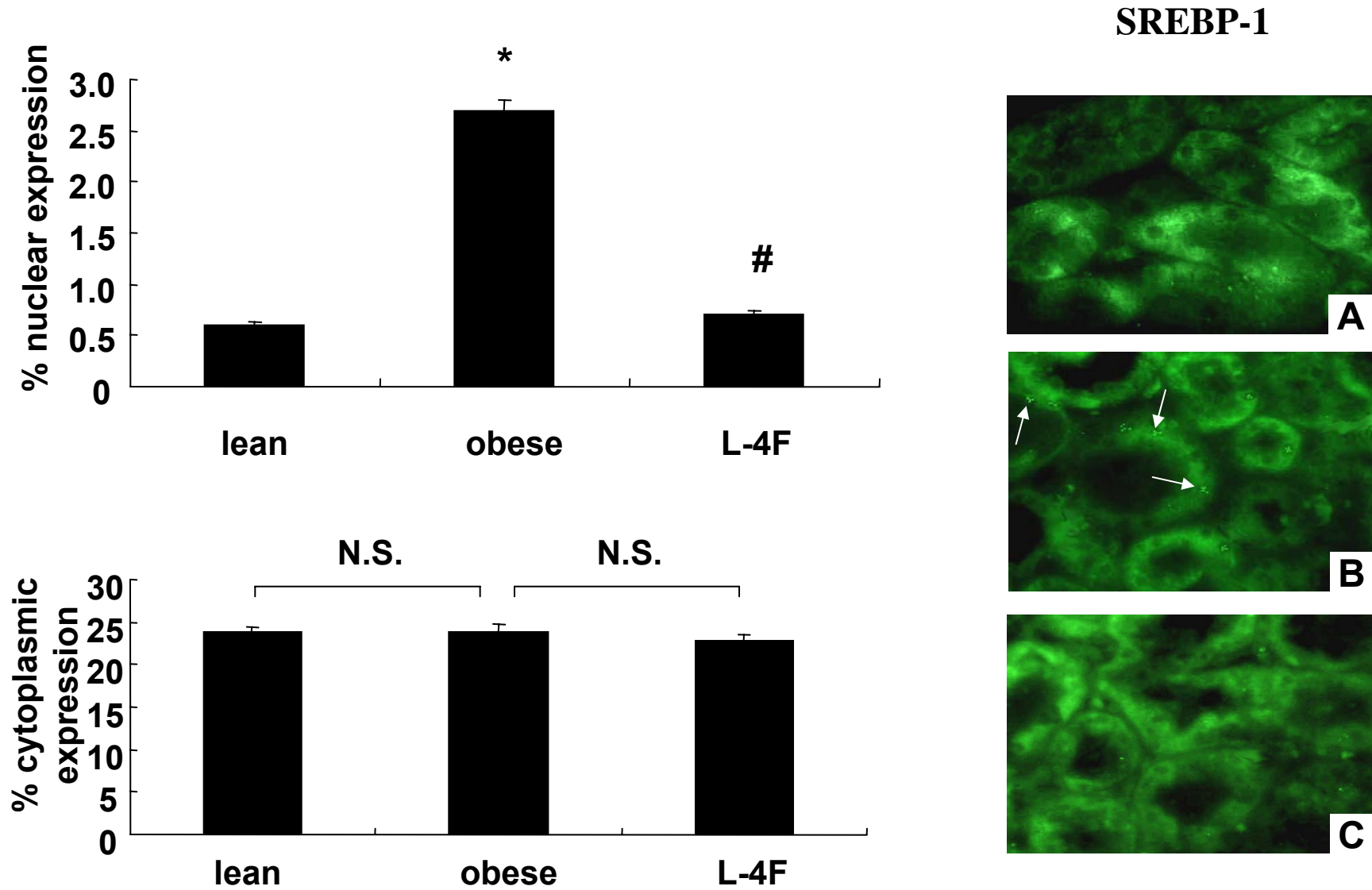
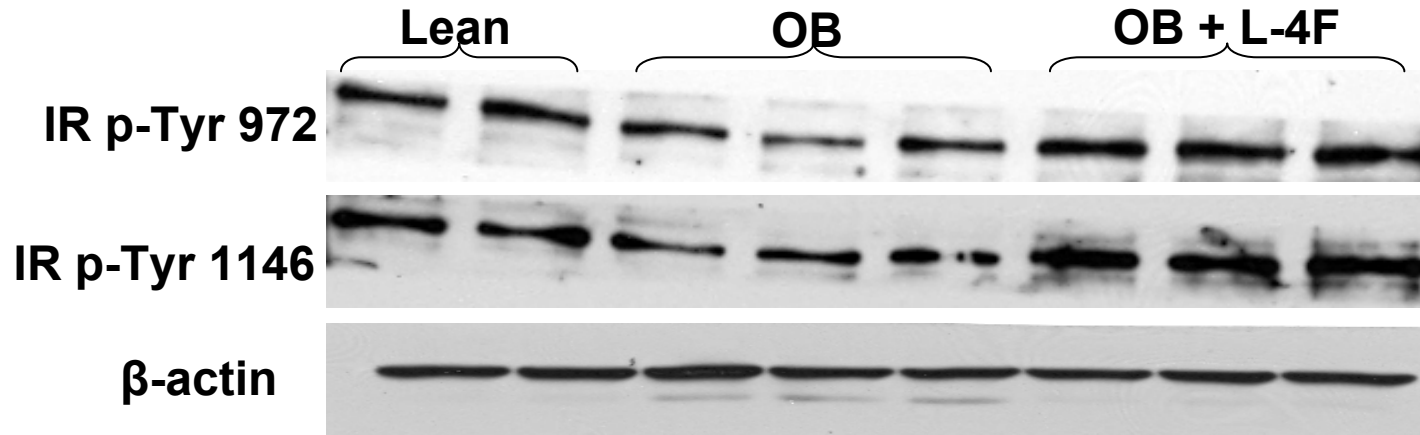


Fig 9

A



B

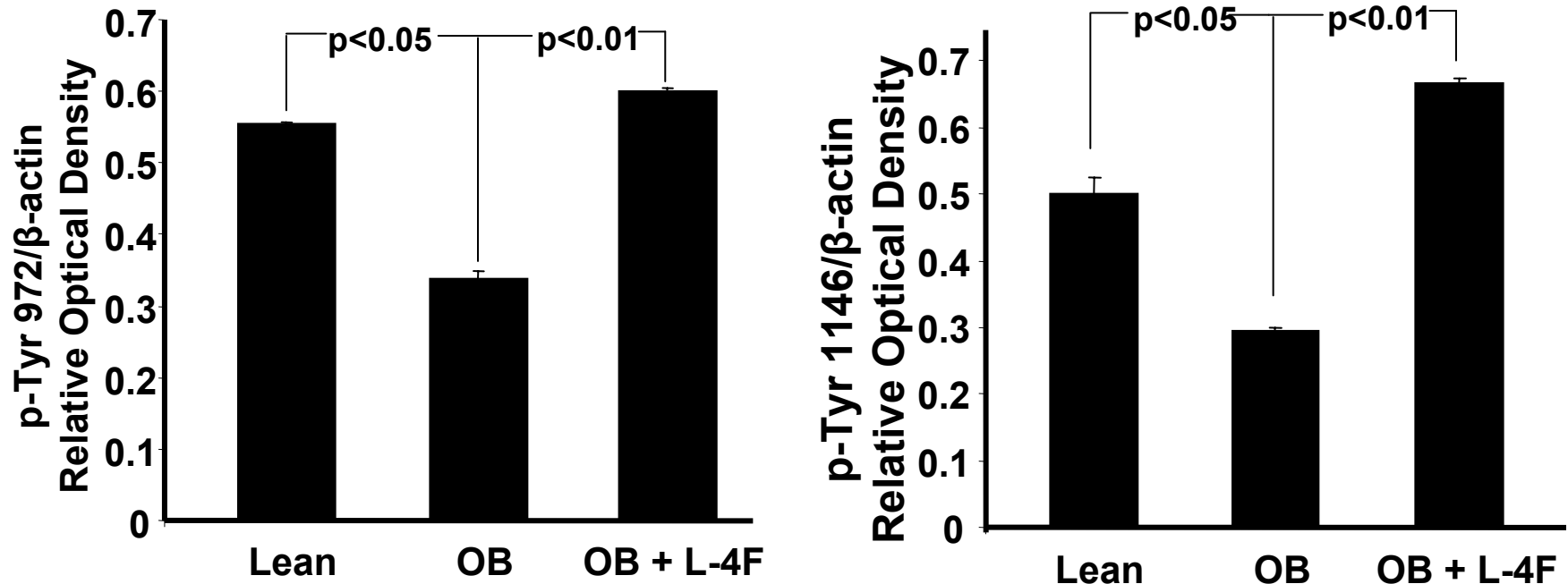


Fig. 10 A

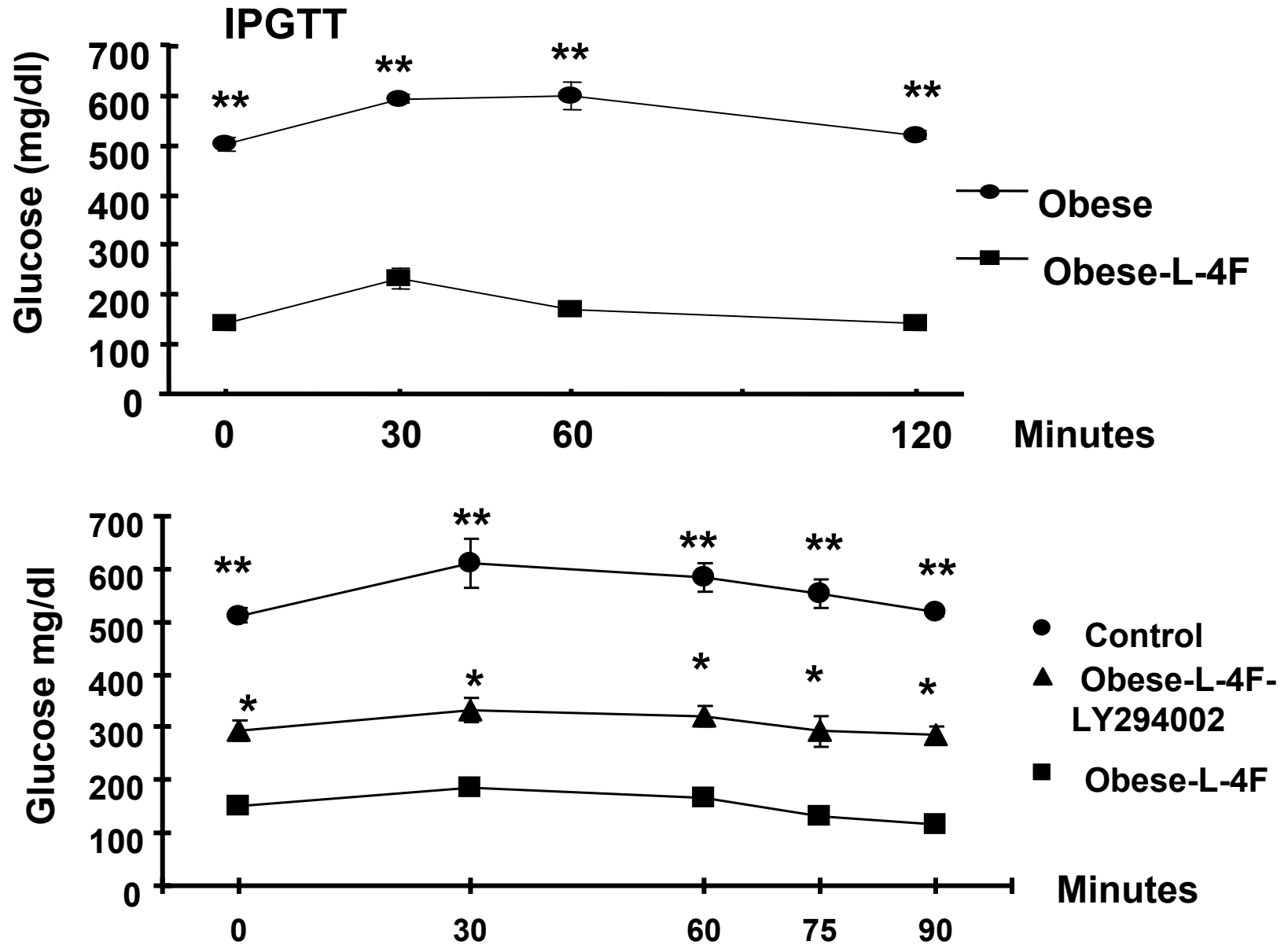


Fig. 10 B

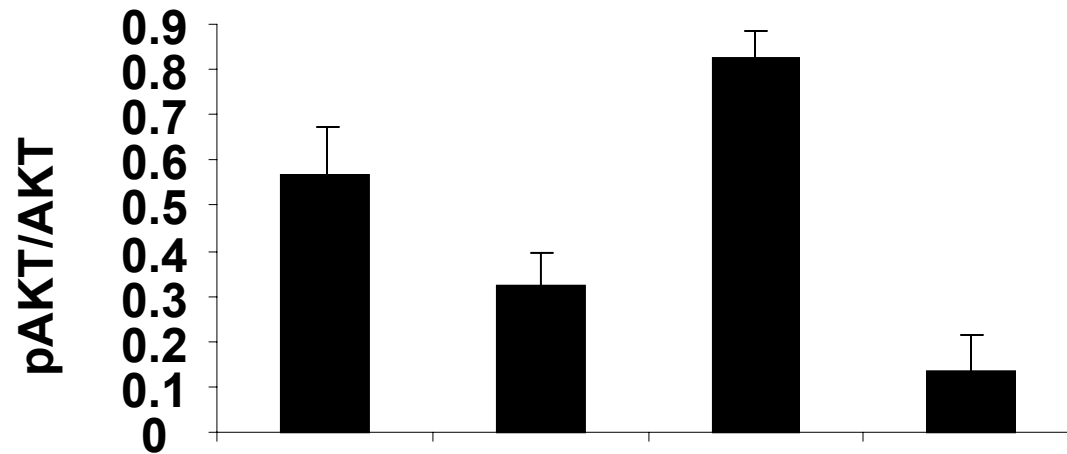
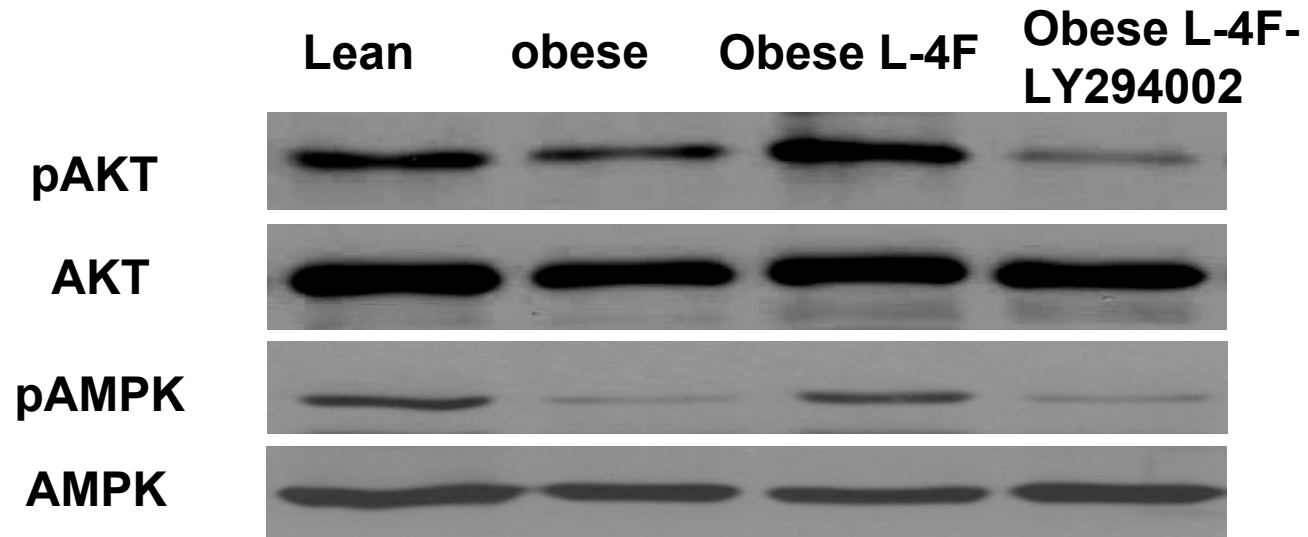


Fig 11

